Stellar population synthesis based on dense grids of detailed binary evolution models

Bachelorarbeit in Physik

von
Sylvia Carmen Désirée Adscheid

angefertigt im
Argelander-Institut für Astronomie

vorgelegt der
Mathematisch-Naturwissenschaftlichen Fakultät

der
Universität Bonn

August 2018

Ich versichere, dass ich diese Arbeit selbständig verfasst und keine anderen als die angegebenen Quellen und Hilfsmittel benutzt sowie die Zitate kenntlich gemacht habe.

Bonn, den. . . . . Unterschrift. . . . . .

1. Gutachter: Prof. Dr. Norbert Langer
2. Gutachter: Prof. Dr. Peter Schneider

Contents

1 Introduction

In this thesis we use a binary star data grid to investigate the influence of binary interaction on certain features of stellar clusters and evolution. Our focus herein lies on binaries with high-mass primary stars ($M_1 \approx 10$–$40\mathrm{M}_\odot$).
The large amount of models allows us to simulate different stellar clusters and examine especially the effect of binary interaction by splitting up the data into interacting and not interacting systems. On this basis we can distinguish those features affected and those unaffected by interaction. We extend our view on binary evolution furthermore by taking into account merger systems. We calculate mass and rejuvination of the merger products and add them back to the data based on models from the grid.
In particular we deal with the unravelling of main-sequence turn-offs and the age-luminosity relation on the red giant branch.

2 Theory

2.1 Evolution of massive stars

This subsection is based on the lecture notes by Pols (2009), unless otherwise noted.
Stars form out of massive molecular clouds collapsing under their own gravity. The gas contracts and heats up internally, gravitational contraction being the energy source, until the temperatures are sufficiently high for nuclear fusion so begin in the core. From this moment on contraction stops and the star settles on the zero-age main sequence.
The luminosity of such a star is highly dependent on its mass M:

$$L \propto M^3 \tag{1}$$

So higher-mass stars are located at much higher luminosities. On the main-sequence stars burn hydrogen in their cores producing helium. In course of this stars with masses higher than $1\mathrm{M}_\odot$ evolve towards lower effective temperatures and higher radii, so they move to the upper right of the main sequence.
Higher-mass stars consume their internal fuel much faster than lower-mass stars and as more massive stars are located at the top of the main sequence the most luminous stars are the first to exhaust hydrogen in their cores. While the helium core begins to contract hydrogen burns in a shell around the core and the outer layers expand. The effective temperature decreases and the star moves away from the main sequence towards the red giant branch.
In clusters stars are assumed to be the same age, because they formed at the same time from the same cloud of gas. In a colour-magnitude diagram of star clusters this mass-main-sequence-lifetime relation shows in form of an upper limit on the main sequence defined by the age of the cluster. As higher-mass stars leave the main sequence early, all stars up to a certain mass have already moved away, because their main-sequence-lifetime is shorter than the age of the cluster. So the turn-off point can be used to determine a cluster's age.
There is however an effect that can be observed in star clusters: So-called blue stragglers "lie along an extension of the main sequence in a region that is brighter and bluer than the turn-off" (Sollima et. al. 2007). They are too luminous and hot to be regular main-sequence stars of the cluster's respective age and are believed to be the result of binary evolution.
The stars that turned off the main sequence move up the red giant branch until helium is ignited in the core and a second core burning phase follows. While lower-mass stars develop degenerate cores, massive stars ($M \gtrsim 8\mathrm{M}_\odot$) subsequently ignite carbon and even heavier elements in increasingly shorter burning phases. When the core is eventually made up of iron, no more energy can be won from nuclear fusion and the core collapses, the star ending in a supernova and compact object.

2.2 Roche-lobe and binary mass transfer

The Roche limit, also called Roche-lobe, is defined by Kopal (1955) as "the largest closed equipotential capable of containing the masses of the two stars" in a binary.
When both stars are smaller than this limit, it is called a detached system. No mass is transferred between them. However, when a star expands in its evolution, the radius might exceed the Roche limit. In course of this overflow mass is transferred from the Roche-lobe filling star towards its companion. This is referred to as a semi-detached system. In case of both stars overflowing their Roche-lobe they form a contact-system with both stars are probably touching each other at the inner Lagrangian point L1 (Kopal, 1955).
When mass transfer occurs unstably and the radius of a mass transferring star does not respond sufficiently fast to the mass loss and continues to overflow its Roche limit, the accreting star can be engulfed by the envelope of the donor (common envelope). In course of this the secondary star loses energy moving through the gas. The energy loss either ends in a spiralling into the primary star and a merger or in expelling the common envelope with the released energy (Merchant, 2016).

3 Methods

For this thesis we use the binary star data grid by Merchant (2016) created with 1D stellar evolution code MESA (Modules for Experiments in Stellar Astrophysics). It contains a multitude of binary models dependent on the parameters $\log(M_1)$ (mass of the primary star), $\log(P/d)$ (orbital period in days) and $q = M_2/M_1$ (mass ratio of the secondary to the primary star). $\log(M_1)$ reaches from 1.0 to 1.6 ($10M_\odot$ - $\approx 40M_\odot$) in intervals of 0.05, $\log(P/d)$ from 0.025 to 3.500 ($\approx$ 1d - $\approx$ 3200d) in intervals of 0.025 and q from 0.025 to 0.975 in intervals of 0.025.
The models provide a full history of the systems' development and are evolved until central carbon depletion (or helium depletion in case of more massive stars) unless certain occurrences during mass transfer cause the calculation to terminate. These include overflowing the Lagrangian point L2, inverse mass transfer with a post-main sequence star, reaching the upper $\dot{M}$ limit (maximal mass loss rate sufficient to expel transferred mass that a secondary star is unable to accrete) and convergence errors. In these cases a merger is assumed to happen. Common envelope evolution results in merger in this grid, too. Even if envelope ejection is possible, this effect is not modelled and we can not take those objects into account.

3.1 Non-interacting systems

Not all systems in the grid undergo mass transfer. Especially for low-mass primary stars, low q and high $\log(P)$ there are binaries without interaction between the stars during their lifetime. These evolve like single stars and we use them to emulate genuine single stars in this thesis.
The non-interaction boundary is the line that sets the limit of $\log(P/d)$ for each $\log(M_1)$ and q pair to interact. If $\log(P/d)$ is higher than the boundary, the system will not interact. Whether a model interacts or not we can determine by examining the Roche-lobe overflow of each star. If overflow happens, mass transfer occurs and the system will count as a interacting system henceforward. However many mass transferring models do not show the Roche-lobe overflow in their actual data history but rather a converging of the star's radius towards the Roche-lobe during transfer. As a result the non-interaction boundary is best reproduced when we set the condition for mass transfer to filling over 99% of the Roche-lobe.
With this method we can determine for each model if and when interaction happens. That allows us to split up models between before-interaction and after-interaction, which is useful to compare systems that transfer mass to those that do not.
Due to the orbital period being limited to $\log(P/d) = 3.5$ there is not a non-interacting system for every binary in the grid, especially for the most massive ones. The most massive non-interacting secondary star has a mass of $17,4M_\odot$, so above this mass we can only examine primary "single stars".

3.2 Mergers

To include merged systems to the data, we use the method by Schneider et al. (2016), which is valid if both stars are in their main-sequence phase when the merger happens, which only applies to about a fifth of the total amount of mergers in the grid. Therefore we can not consider post-main-sequence mergers in this thesis. We identify mergers in the grid by comparing the time of termination of both stars in each binary. If the point of time is the same it is a merger. The mass of the merger product is then calculated using

$$M = (1 - \Phi)(M_1 + M_2) \tag{2}$$

with $\Phi = 0.3q/(1+q)^2$ the mass lost in the merging process. Here q refers to the mass ratio at the moment of the merger and not the initial ratio. To be able to describe the product with data from the grid we abandon all those which have a calculated mass higher than $40\mathrm{M}_\odot$.
To calculate the rejuvination of the merger product it is necessary to know which mass M, hydrogen mass fraction X and age τ_{MS} the progenitor stars would have at the end of main sequence. For each star we take these information from the long-period "single star" equivalents above the non-interacting boundary. For the models without such an equivalent we receive the quantities needed by interpolating between those of the available "single stars".

$$Q_m = \frac{M_{\mathrm{ini}} - M_{\mathrm{TAMS}}}{M_{\mathrm{ini}}} \tag{3}$$

$$Q_c = \frac{X_0 - \langle X \rangle_{\mathrm{TAMS}}}{X_0} \tag{4}$$

With these properties it is possible to calculate the mass lost on main sequence Q_m, the effective core mass fraction Q_c and fractional main sequence age f. The apparent fractional main sequence age in then determined using

$$f_{\mathrm{app}} = \frac{f_i}{\alpha} = \frac{1 - \langle X \rangle / X_0}{\alpha Q_{c,i}} \tag{5}$$

with $\alpha = 1.14$ and

$$\frac{\langle X \rangle}{X_0} = \frac{(1 - Q_{m,1} f_1)(1 - Q_{c,1} f_1 - \Phi)}{(1-\Phi)[(1 - Q_{m,1} f_1) + (1 - Q_{m,2} f_2) q]} + \frac{(1 - Q_{m,2} f_2)(1 - Q_{c,2} f_2 - \Phi) q}{(1-\Phi)[(1 - Q_{m,1} f_1) + (1 - Q_{m,2} f_2) q]} \tag{6}$$

$Q_{c,i}$ and $Q_{m,i}$ of the merger product we receive through interpolation again. Finally the "initial mass" M_i of the merger product can be calculated:

$$M_i = \frac{M}{1 - Q_{m,i} f_i} \tag{7}$$

The error on determining M_i caused by the interpolation is higher for more massive merger products and amounts to about 0.7% for the most massive.
With the apparent initial masses of the mergers known we assign each one to a non-interacting "single star" model from the grid which most closely resembles its initial mass. Due to the characteristics of the non-interaction boundary only primary star models are available for this in cases of masses higher than $17.4\mathrm{M}_\odot$ which leads to a strong discretisation above this threshold. As a consequence the error on assigning the merger products to models amounts up to 5.7%, which is much higher than the error resulting from the interpolation. Masses higher than $40\mathrm{M}_\odot$ again are abandoned. This leaves about 15.4% of the total amount of mergers available for further investigation.
With the mergers assigned to "single star" models and the apparent age and real age known we include these models to our data from the evolutionary point of time of their apparent age at the corresponding real age. It needs to be noted that the assigning leads to the merger models behaving like single stars which were formed as such. Changes in internal properties (such as rotation) in result of the merging process can therefore not be emulated using this method and remain unconsidered in our further analysis.

3.3 Weight

To emulate actual abundances of different kinds of stars the data in the grid need to be weighted. In doing so we intent to receive evidence of the likeliness to observe certain systems.
We weigh each system by the initial mass function of the primary star (Sana et al. 2013)

$$f(M_1) \propto M_1^{-2.35} \tag{8}$$

and by mass ratio and orbital period (Sana et al. 2013)

$$f(q) \propto q^{-0.1} \tag{9}$$

$$f(\log(P/d)) \propto \log(P/d)^{-0.55} \tag{10}$$

So through the weighting of the data we favour systems with lower masses and mass ratios and closer binaries.

3.4 Hertzsprung-Russell diagram

As the grid provides for each model a full history of luminosity L and effective temperature T_{eff} development, we use these to compress large amounts of data and make them visible in form of a Hertzsprung-Russell diagram (HRD), which gives a graphic overview of evolution and an impression of what observational data (colour-magnitude diagram) might be expected.
To consider the weighting of the models we depict these as a coloured density map rather than a scatter plot. That enables to make a statement on how populated certain regions of the HRD are. To make them comparable to each other the density index for diagrams showing similar issues needs to be set to a fixed value. This is necessary, because discretisation causes single distinct patches to be much more populated than the rest of the plot and not setting an upper limit for density would cause the final images to show only these points, everything else being too faint to be seen.
To emulate regions of constant star formation we iterate through all models' histories and set L-T_{eff} points in intervals of 10,000 years. Star clusters of the same age are generated by setting only one point per star at the point of time closest to the respective age.

4 Results

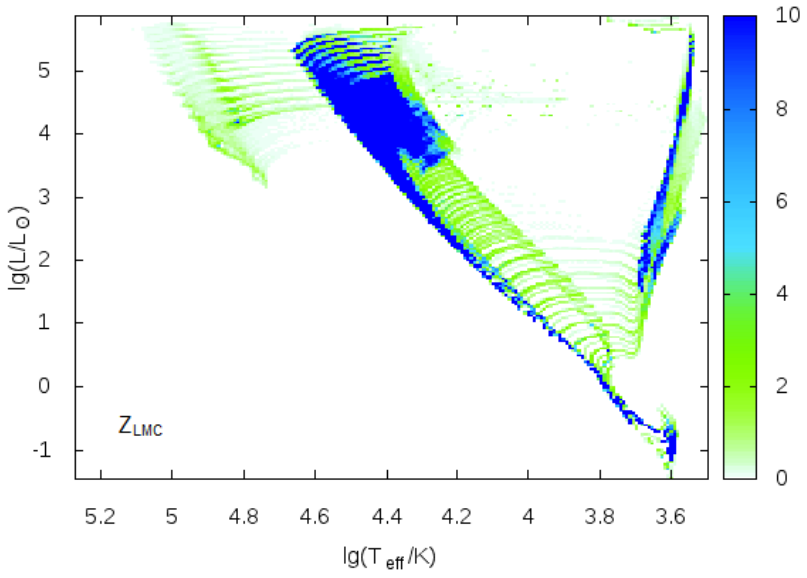

Figure 1: HRD as a density map for constant star formation, containing all models in the data grid plus calculated mergers. All models are weighted according to section 3.3. The density index is limited to 10 for better visibility of faint features.

Figure 1 shows the HRD for the evolution of all models in the grid as well as merged stars. It gives an overview of main-sequence (MS) in the middle and red giant branch (RGB) on the right. However, in this depiction no details are visible. As our focus lies on high mass stars it is sufficient to depict the upper end of MS and RGB which is where these objects are primarily located.
Figure 2 and 3 show those cut-outs.
To investigate which role binary interaction plays in the evolution of stars in the grid, we split the data up into three components: Stars that have interacted with their companion (i.e. transferred mass), stars that have not done so and mergers. The diagrams for each separate component are depicted in the appendix in Figure 22 to 24 for the MS and in Figure 25 to 27 for the RGB.

The cut-out in Figure 2 shows predominantly discretised main-sequence evolution of non-interacting stars and merger products. Interacting stars appear in the overall picture as a comparatively blurred background on the MS. However, interacting stars add two visible features: The first is a widening of the MS towards lower temperatures by $\Delta \log(T_{eff}/K) \approx 0.05$. Section 4.1 shows that this is caused by mass accretion of secondary stars at the MS turn-off. The second feature is a total of 13 extensions of the MS towards higher temperatures and luminosities. 13 is the number of discrete primary masses in the data grid and these extensions can be identified as primary stars that strip off their hydrogen-rich envelope in mass transfer and move towards the helium main-sequence.
On the RGB in Figure 3 non-interacting systems and mergers, as well as on the MS, show a single-star-like evolution. Interacting systems again blur the discretisation. Additionally they cause the red giant branch to extend towards higher temperatures, causing a doubling of the visible width in a range of $\log(L/L_{\odot}) \approx 4.6$–$5.2$. In Section 4.2 the relation between luminosity and age on the RGB are investigated.

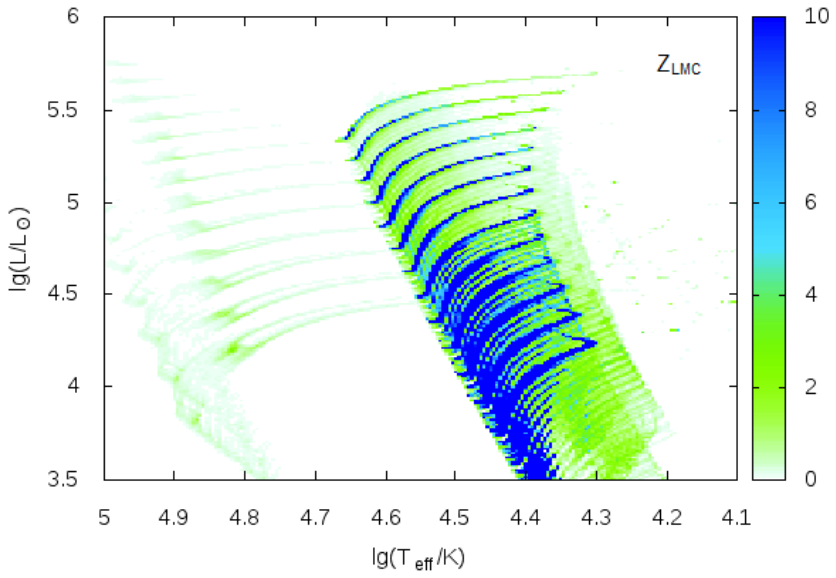

Figure 2: HRD as a density map for constant star formation, containing all models in the data grid plus calculated mergers. Depicted is only the upper end of the main-sequence. All models are weighted according to section 3.3. The density index is limited to 10 for better visibility of faint features.

Figures 4 and 5 show the intensity of all three components as a function of luminosity for the upper MS and RGB.
The MS is strictly dominated by the non-interacting systems in whose peaks primary star mass discretisation is visible. This seems likely as stars spend most of their lifetime in this phase and many interactions take place towards the end of it or afterwards when stars expand and fill their Roche-lobe. As a result interacting systems have a (at their maximum) ten times lower intensity than non-interacting systems.
Intensity decreases with increasing luminosity due to the weighting by the initial mass function favouring lower primary masses. Mergers are also affected by this, but the maximum lies at higher luminosities, because merging produces stars of higher mass than their primary predecessor but with their weighting. The merger products have a seemingly too high weight for their respective mass. So the intensity maximum is shifted towards higher luminosities.
On the RGB non-interacting systems are even steeper in terms of peaks caused by discretisation. But despite these peaks they are not absolutely dominant anymore. As many interactions take place before a star reaches the RGB the ratio of non-interacting systems strongly decreased compared to interacting systems and mergers.
Weighting again causes a decrease towards high luminosities. Mergers dominate the upper end of the branch. Here we see the discretisation, too, which originates from assigning the merger masses to "single star" models.
So we see that binary interaction has an overall larger effect on the red giant branch than it has on the main sequence.

4.1 Star clusters and the unravelling main-sequence turn-off

Figures 28 to 32 in the appendix show HRDs at five different constant times, simulating clusters in which all stars are the same age. They include both interacting and not-interacting systems but

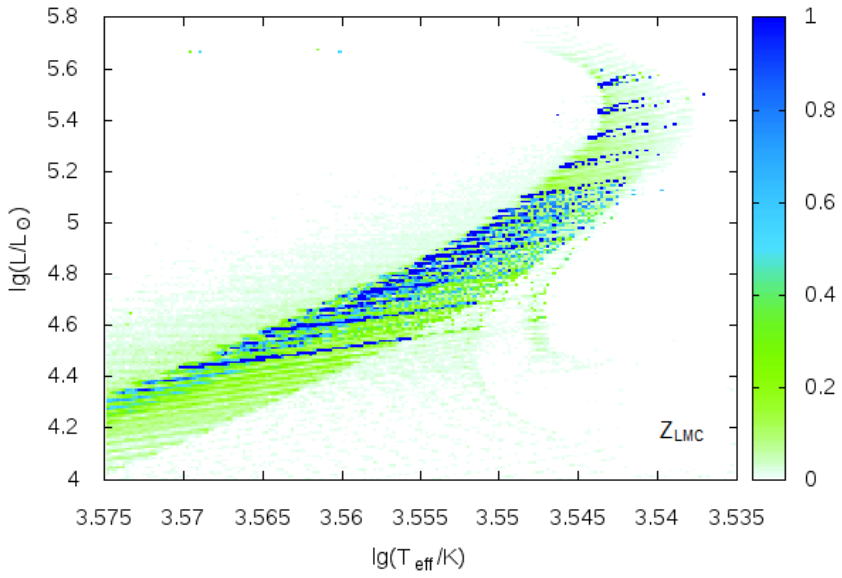

Figure 3: HRD as a density map for constant star formation, containing all models in the data grid plus calculated mergers. Depicted is only the upper end of the red giant branch. All models are weighted according to section 3.3. The density index is limited to 10 for better visibility of faint features.

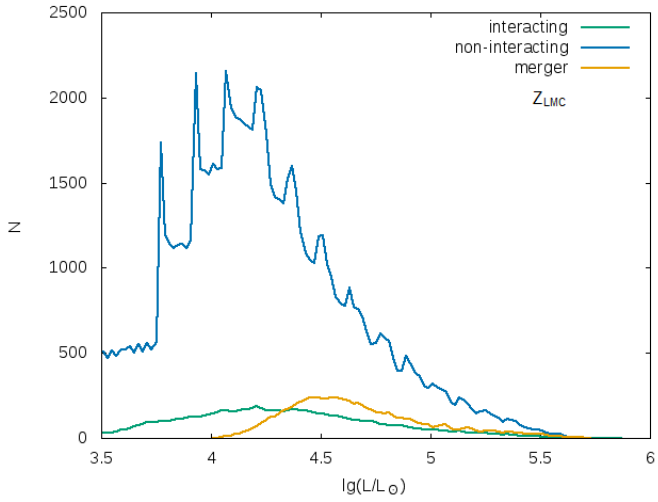

Figure 4: Histogram of the upper main-sequence cut-out as seen in Figure 2. Intensity is plotted as function of luminosity each for interacting systems, non-interacting systems and mergers. All models are weighted according to section 3.3.

.

no merged ones. Those are added to the data in Figures 33 to 37.
What one can see is a typical main-sequence turn-off, that indicates the cluster's age, moving down the MS over time towards lower luminosities and temperatures. However, one can see a noticeable feature: The turn-off unravels into a total of four distinct branches which are more populated than

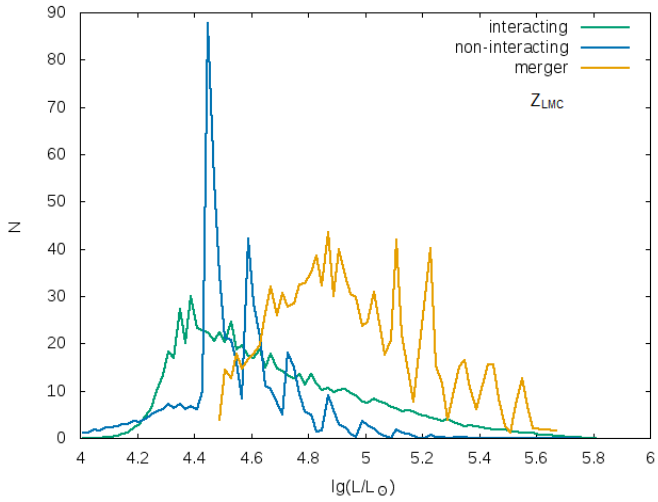

Figure 5: Histogram of the upper red giant branch cut-out as seen in Figure 3. Intensity is plotted as function of luminosity each for interacting systems, non-interacting systems and mergers. All models are weighted according to section 3.3

their surrounding area. This is best visible in Figures 29, 30 and 31. These branches are different from each other in terms of intensity so the plots' density scale (colour index) is limited to an upper value at which all branches are clearly distinguishable.

In the following we will examine each branch so Figure 6 shows them each with a number for identification.
One can see the following:

- Branch 1 on the middle left is the most populated one. It is the regular main sequence turn-off where mainly the models that have not yet interacted reside and begin to evolve away from the main sequence. This line is highly affected by discretisation, so single, very populated points lead to a massively increased intensity especially for stars at lower primary star masses as they are favoured by the initial mass function.
- Branch 2 is located to the left of the turn-off point at higher temperatures and luminosities. This is where we might expect to find blue stragglers.
- Branch 3 on the middle right runs parallel to the actual MS turn-off but at lower temperatures, forming a "redder turn-off". The width of the gap between both branches is about the same for all clusters in Figures 28 to 32: $\Delta \log(T_{eff}) = 0.05 \pm 0.003$. This branch causes the widening of the main sequence observed in Figure 2.
- Branch 4 on the far right is comparatively short and splits from branch 3.

The difference in intensity of all four branches is illustrated by Figure 7. It shows the intensity in an interval of range $\Delta \log(L/L_\odot) = 0.1$ as a function of temperature for five different cluster ages. To get a slim peak for each branch we choose an interval at which the branches are as vertical and intense as possible whilst avoiding the distinct patches affected by the discretisation of primary star mass as these are disproportionately overpopulated. The rightmost branch 4 never gets vertical, but it has a high intensity in the interval where branches 1 and 3 become vertical. The intervals for each time are listed in Table 1. The intensities for each separate branch can be seen in Figures 8 to 11. As branch 2 reaches its best verticality and intensity at higher luminosities than the other branches we choose different intervals for Figure 9 which are listed in Table 2.
The regular turn-off on branch 1 has a higher intensity than the other three at all times. This

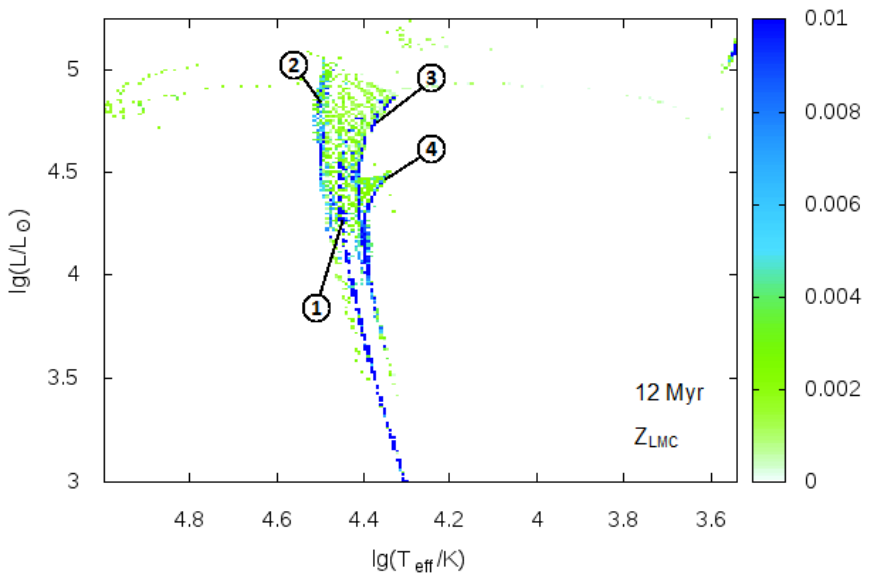

Figure 6: Density map HRD of the main-sequence turn-off of a star cluster at constant age 12Myr, containing interacting and non-interacting systems. All models are weighted according to section 3.3. The density index is limited to 0.01 for better visibility of faint features. The labels serve for identification of the distinct branches. See text for explanation of the labels.

is explained by Figure 8 which shows that the upper MS is highly dominated by non-interacting stars and in our clusters these are located in the regular turn-off.
All branches have in common that their intensity at first increases with age reaching a maximum at about 18Myr and decreasing afterwards. Figure 8 can explain this behaviour, too. The weighting favours stars at the lower end of the primary mass range and suppresses the higher end. As higher-mass stars reach the end of MS earlier the younger turn-offs have lower intensities. With lower masses and therefore higher ages intensity increases. However, the older the clusters get the less models remain in total and there are no more primary stars below the lower limit of $10M_{\odot}$, so intensity decreases again with increasing age.
The effect of lessening model numbers is especially reflected by the 30Myr old cluster. The data in Figure 32 is very granular and branch 4 is hardly recognisable as such. Additionally, the little of model numbers causes each patch to have a larger impact: In Figure 10 branch 3 seemingly increases in intensity again for the age of 30Myr. The reason for this is a single overpopulated patch located in the plotting interval despite the branch having an overall lower intensity at this age.

In the following we investigate the origin of each branch. For this first we plot an HRD for a cluster with the data divided into primary and secondary stars (see Figure 12). It is a scatterplot rather than a density map as it enables to colour each point by certain features. We choose an age of 10Myr, because from this time on all branches have a clear visibility and the total number of models is still high.
From Figure 12 one can see: Branch 4 is exclusively populated by primaries while only secondaries reside on branch 2 and 3. Primary stars form not only branch 4 but also a small accumulation and a distinct line below.

Split upper main sequences have been observed in a variety of clusters and it has been suggested

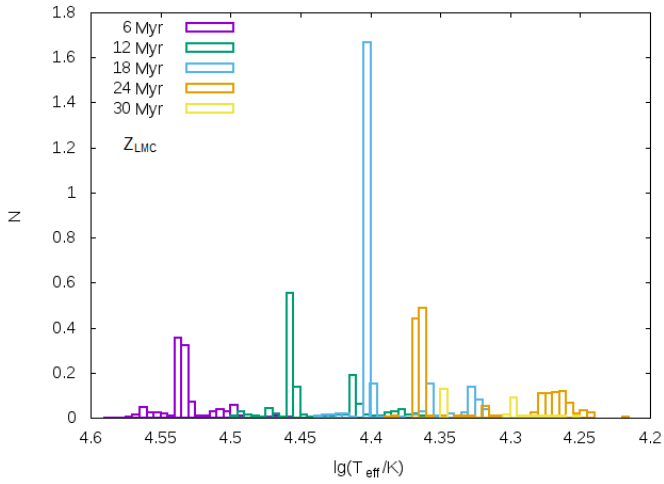

Figure 7: Histograms of the intensity development of the four branches in Figure 6 over time in the luminosity intervals in Table 1.

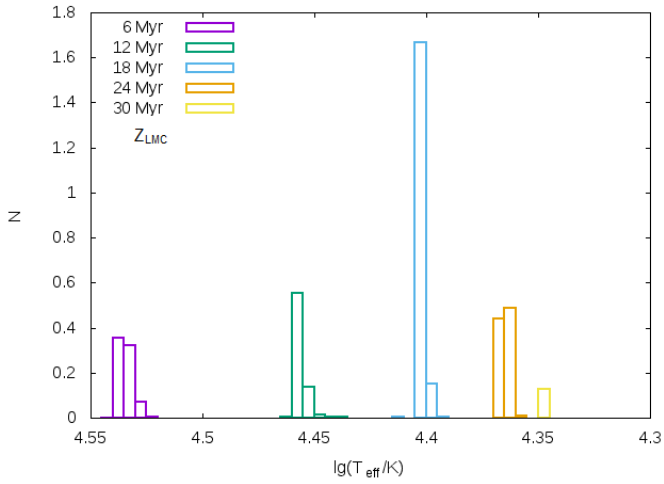

Figure 8: Histograms of the intensity development of branch 1 in Figure 6 over time in the luminosity intervals in Table 1.

that the red MS consists of rapidly rotating stars, the blue MS of slowly or non-rotating stars, the latter possibly being formerly fast rotators that were braked (D'Antona et. al. 2017; Milone et. al. 2018).
To investigate if this might be the reason for unravelling turn-offs in our figures, we plot primary and secondary stars individually and colour the dots according to their rotational velocity at the equator: Figure 13 and .14.

The primary stars do not show a special behaviour in terms of rotation. Most of them are rather slow rotators ($v_{rot} \lesssim 200$km/s), the slowest ones being located on the regular MS turn-off. The secondary stars however show: The redder turn-off in branch 3 consists of fast rotators ($v_{rot} \approx 300$–600km/s) while the blue branch 2 consists mainly of rather slow rotators compared to that ($v_{rot} \approx 100$–200km/s).
A close examination of the models located in branch 3 reveals: It contains stars which have ac-

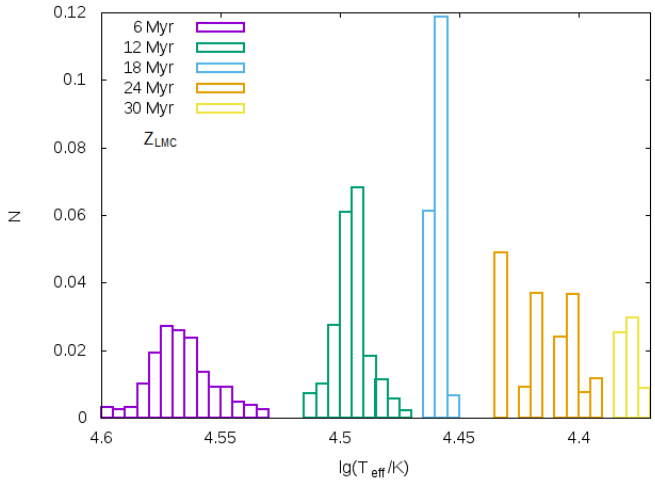

Figure 9: Histograms of the intensity development of branch 2 in Figure 6 over time in the luminosity intervals in Table 2.

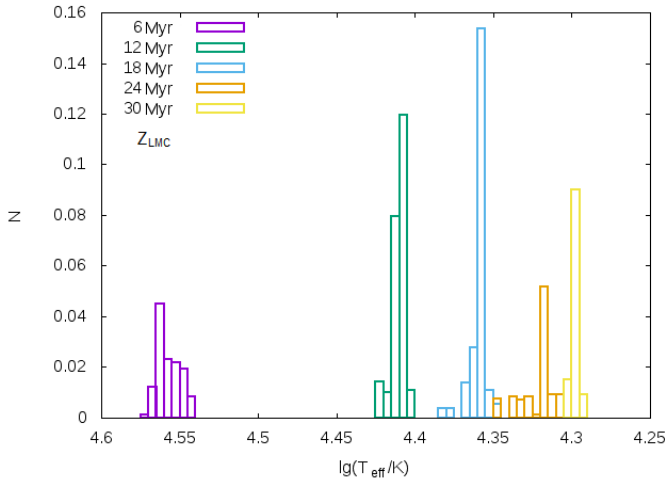

Figure 10: Histograms of the intensity development of branch 3 in Figure 6 over time in the luminosity intervals in Table 1.

creted mass from their companion and spun up by transferred angular momentum. In the course of this the stars expand a bit and undergo a slight temperature drop which is reflected by the gap between the red and the regular turn-off. Towards higher luminosities the stars in this branch slow down again as their are in the end of their main sequence phase and as such expanding. To conserve angular momentum this requires a decrease of rotational velocity.
To investigate the slower rotating branch 2 it is useful to split up the secondary stars into those which do not have a companion star anymore (Figure 15) and those which still have one (Figure 16). Because from these diagrams one can see that branch 2 is not homogeneous but actually consists of two different features: Stars on this branch that have lost their primary companion form a parallel line to the red turn-off while stars that are still in a binary form a clump in the blue straggler area. This clump in itself has at least three regions of higher density than the surrounding. They can be seen best in Figure 12. To understand the origin of those features we look at several sample stars from each one and their development over time. The examples are listed

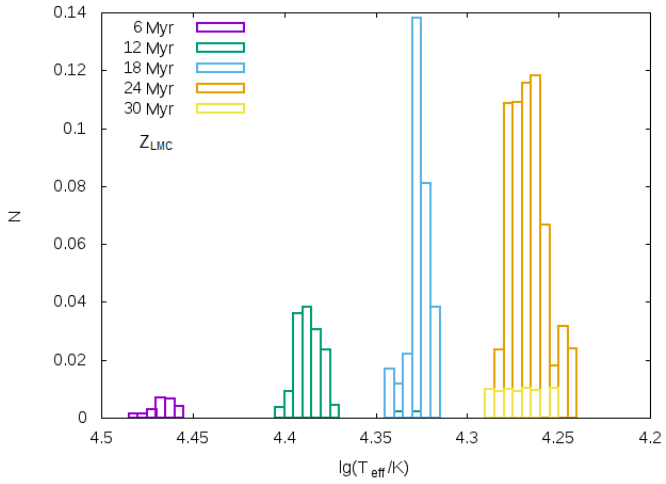

Figure 11: Histograms of the intensity development of branch 4 in Figure 6 over time in the luminosity intervals in Table 1.

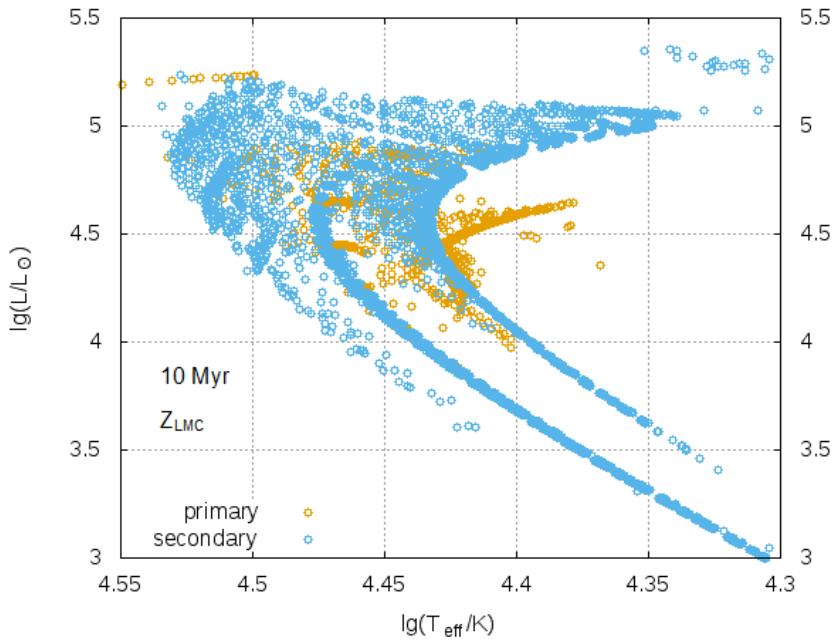

Figure 12: Scatterplot HRD of the main-sequence turn-off of a star cluster at constant age 10Myr, containing interacting and non-interacting systems. Orange points are primary stars, blue points are secondary stars.

in Table 3.
It turns out that the sample stars on the slow-rotating parallel in Figure 15 all have certain things in common: They are all former companions of stars at the upper end of our primary star mass range (M_1) $\gtrsim 28M_\odot$) with a low mass fraction ($q \leq 0.475$) and a short orbital period ($P \lesssim 2$d). They undergo several highly non-conservative mass transfers being spun up rapidly and braked subsequently so the overall change in rotational velocity compared to the initial value is rather

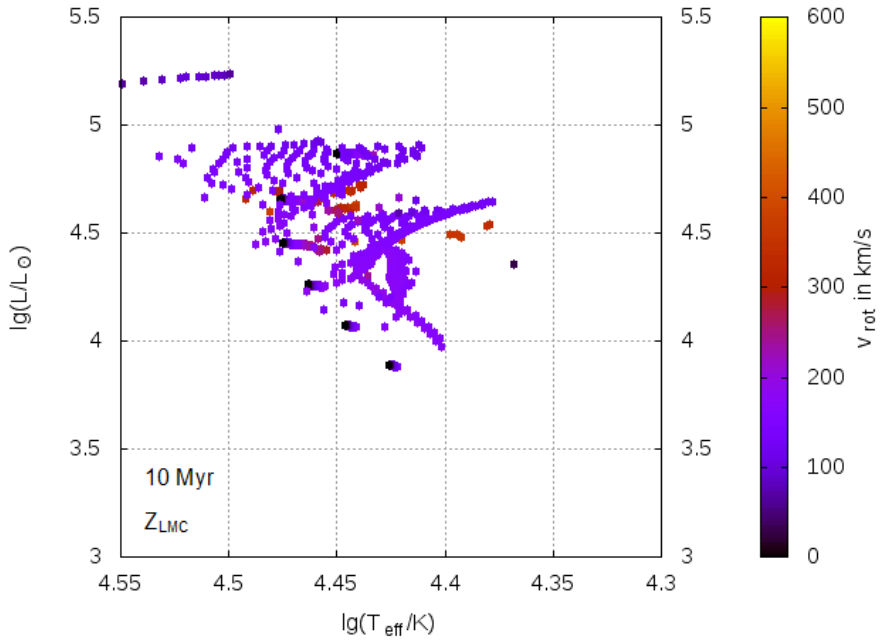

Figure 13: Scatterplot HRD of the main-sequence turn-off of a star cluster at constant age 10Myr, containing interacting and non-interacting systems. Only primary stars are depicted. The colour of the points indicate the equatorial rotational velocity of each star.

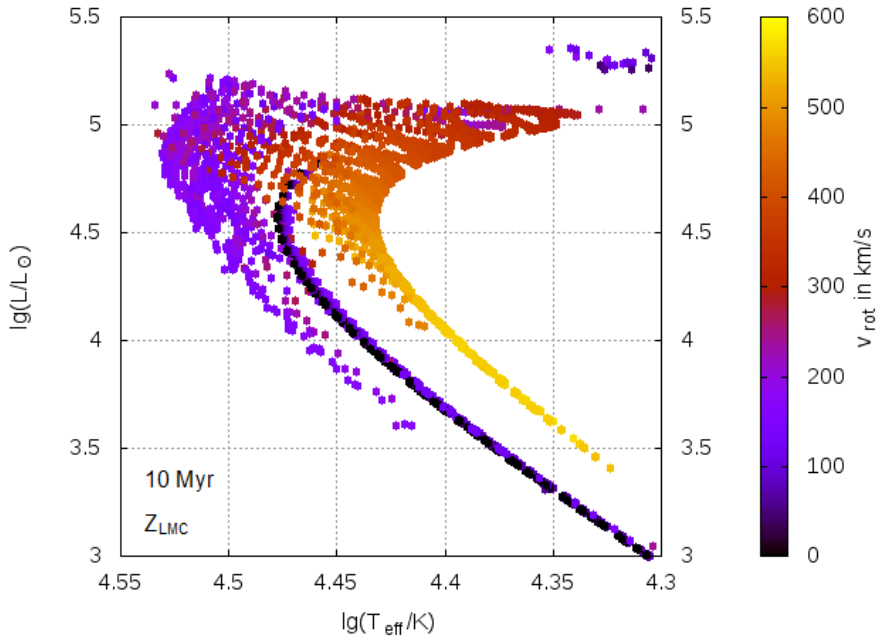

Figure 14: Scatterplot HRD of the main-sequence turn-off of a star cluster at constant age 10Myr, containing interacting and non-interacting systems. Only secondary stars are depicted. The colour of the points indicate the equatorial rotational velocity of each star.

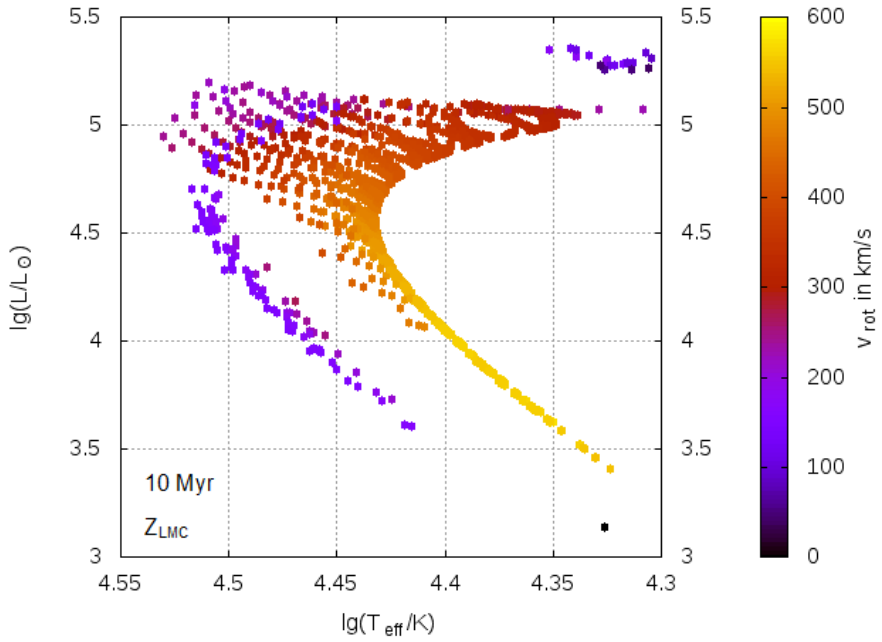

Figure 15: Scatterplot HRD of the main-sequence turn-off of a star cluster at constant age 10Myr, containing interacting and non-interacting systems. Only secondary stars that do not have companion anymore are depicted. The colour of the points indicate the equatorial rotational velocity of each star.

small ($\Delta v_{rot} \lesssim (50 \pm 20)$km/s).
The sample stars in the clump in Figure 16 show a very different behaviour: They are companions of stars in the lower half of our primary mass range ($M_1 \lesssim 18 M_\odot$) with high mass ratios ($q \geq 0.775$) but also a short orbital period ($P \lesssim 2.5$d). They go through a fast mass transfer with their primaries in course of which the mass ratio is inverted, the formerly lower mass star being the more massive, luminous and hotter one afterwards. The secondary is spun up during this process and slows down again afterwards. The fast mass transfer is followed by a long lasting phase of slow mass transfer from the now less massive primary to its companion. These transfers are mostly conservative. In all models the last phase eventually ends in a merger.
The secondaries in this clump have another significant feature: Observing the primary stars with which they are twinned reveals that those are just the stars that make up branch 4, which we have found out to be composed only of primaries in Figure 12. Moreover, investigating the development of those stars over time shows that certain regions of branch 4 are associated with certain dense regions of the clump in branch 2: While the primaries reside on the line below branch 4 after the first mass transfer and move through the small accumulation below into the branch itself with time, the secondaries move upwards through the three dense regions in the clump at the same time. Figures 38 to 40 in the appendix show an example of this on the basis of a binary for whose stars the evolutionary tracks are included into the HRDs of three star clusters of different ages with the current position of both stars each being marked by a red square.
The development of these binaries suggest the possibility that they might be so-called Algol variables, which are semi-detached systems in which the larger, less massive and luminous component lies above the main sequence filling its Roche-lobe transferring mass while the accreting, more massive and luminous component is still on the main sequence (Erdem and Öztürk 2014; Kopal 1955). These systems are believed to originate from binaries in which the lobe-filling star was more massive at first but transferred material rapidly and ended up being the less massive component (Chen et. al. 2003). This definition fits our observations quite well despite the less massive star

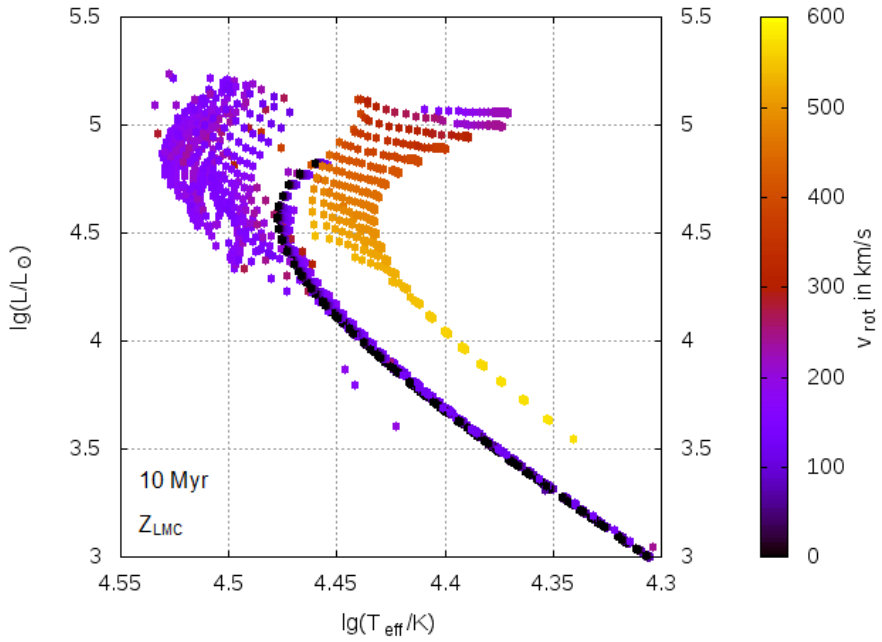

Figure 16: Scatterplot HRD of the main-sequence turn-off of a star cluster at constant age 10Myr, containing interacting and non-interacting systems. Only secondary stars that still have a companion are depicted. The colour of the points indicate the equatorial rotational velocity of each star.

being the larger one only in about half of the investigated models.

This might give a hint at the possible position of Algol-type binary stars in cluster HRDs. A comparison with observational data would be advisable to prove or disprove this assumption. Identifying those stars in actual colour-magnitude diagrams however might turn out to be difficult, not only because these are close binaries and actual temperature and luminosity of each star need to be distinguished from each other to put them on the correct position in the diagram, but also because the respective branches are very low in intensity compared to the main sequence (see Figure 7) and are most likely overlain by other features. Especially the region in which the secondary stars reside is populated by stars of other types as well.

Another type of stars located there are merged stars. They are added to the cluster data in Figures 33 to 37. As they are rejuvinated compared to their real age, they are located at higher luminosities to the left of the turn-off where we would expect them as blue stragglers. In the two youngest clusters discretisation highly affects the image, because high-mass stars evolve fast and therefore interact early, creating massive mergers for which we have only few "single star" models to assign them to. So they form lines in Figure 33 and 34. Towards older clusters and therefore less massive mergers (Figure 35, 36 and 37) we see them form a plane-like accumulation.
The merger models have a lower-mass-limit, because we only have primaries down to masses of $10M_{\odot}$ and therefore no merger products below this mass exist under the given restrictions (see Section 3.2). This causes the merger accumulation to seemingly move away from the turn-off region, but the data simply does not provide new mergers to fill the space in between.

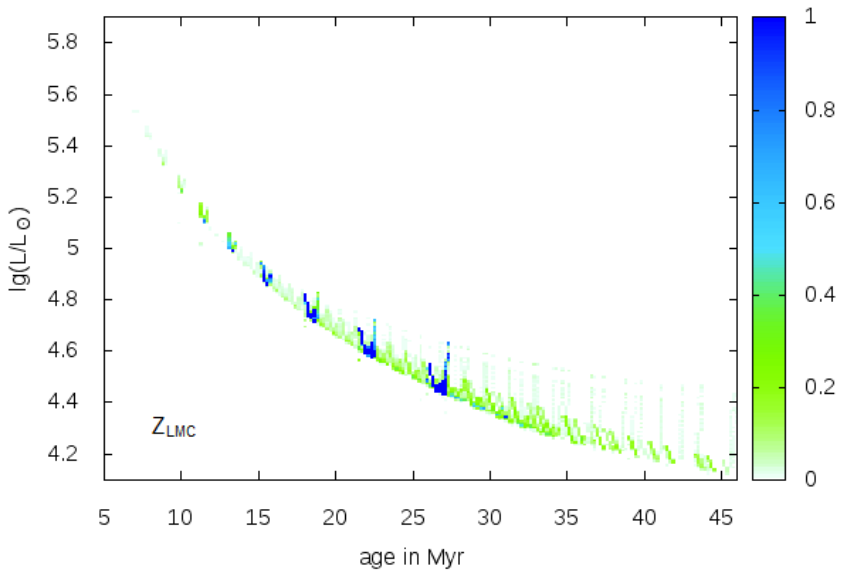

Figure 17: Density map of the luminosity-age dependence on the red giant branch. Depicted are only systems that did not undergo mass transfer. The density index is limited to 1 for better visibility of faint features.

4.2 Luminosity-time dependence on the red giant branch

To investigate the relation between age and luminosity on the red giant branch (RGB) we use the same data as in the HRD cutout in Figure 3 but plot it in dependence of time rather than temperature. Figures 17 to 19 show the diagrams for non-interacting systems, interacting systems, mergers and all of them combined.
One can see that luminosity describes a continuously dropping curve. Massive, short-lived stars are located at high luminosities. The less massive, less luminous stars spend more time in this phase and cause the curve to level out at higher ages. Additionally less massive stars show a steep increase in luminosity at the end of their RGB phase. This happens when helium becomes depleted in the core and carbon burning begins, the latter being only modelled for less massive stars in the grid.
The non-interacting models in Figure 17 show a narrow curve in which the discretisation of the primary star masses is clearly visible in the distinct, most populated patches. The after-interaction models in figure 18 show an overall very similar picture. Mass transfer has blurred the discretisation and so caused the curve to become continuous. The curve is also widened towards lower luminosities in a range from 5Myr to 30Myr. In the middle of this range the widening becomes maximal, the total width of the curve being doubled compared to only non-interacting stars.

Now we take into account the merger systems (see figure 19). Merging forms massive stars which appear younger than they really are, which places the merger products clearly above the luminosity curve in our diagram. They appear to be "too luminous" for their respective age.

Striking about the mergers is the shape that they cover in the diagram. This can be traced back to the calculation of merger mass and rejuvination, especially to the mass ratio q at the time when the merger happens. Figure 20 shows the relation of primary and secondary mass at the moment of merging and figure 21 shows the outcome in the final luminosity-age plot. It is possible to identify certain properties of both depictions with each other. These are labelled with numbers

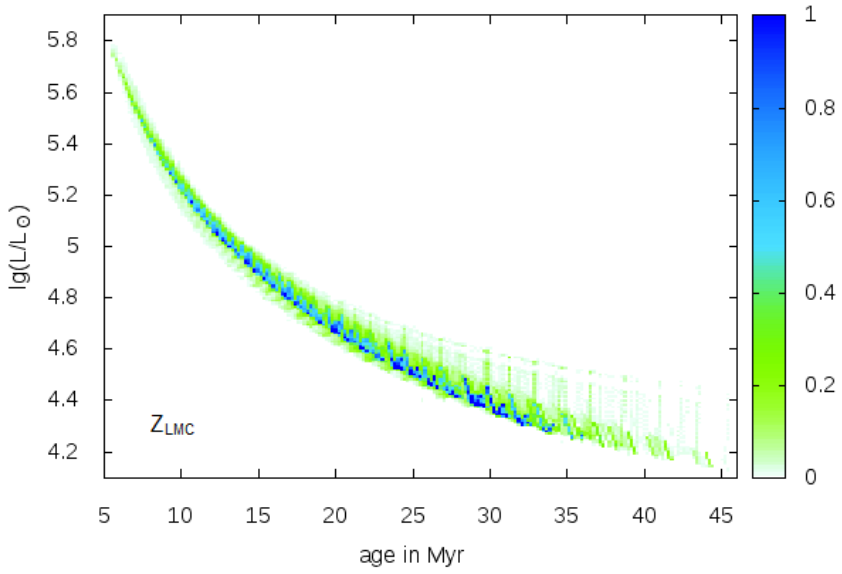

Figure 18: Density map of the luminosity-age dependence on the red giant branch. Depicted are only systems that did undergo mass transfer. The density index is limited to 1 for better visibility of faint features.

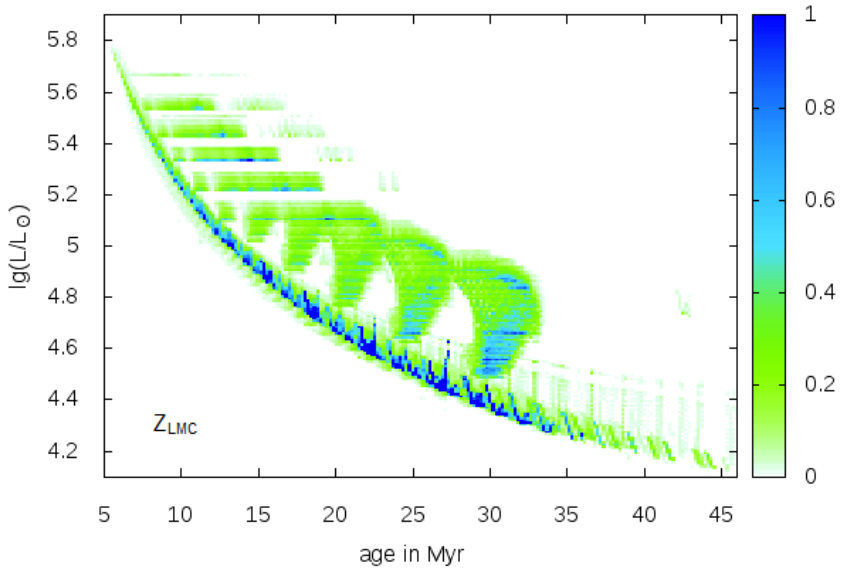

Figure 19: Density map of the luminosity-age dependence on the red giant branch. Depicted are all systems plus mergers. The density index is limited to 1 for better visibility of faint features.

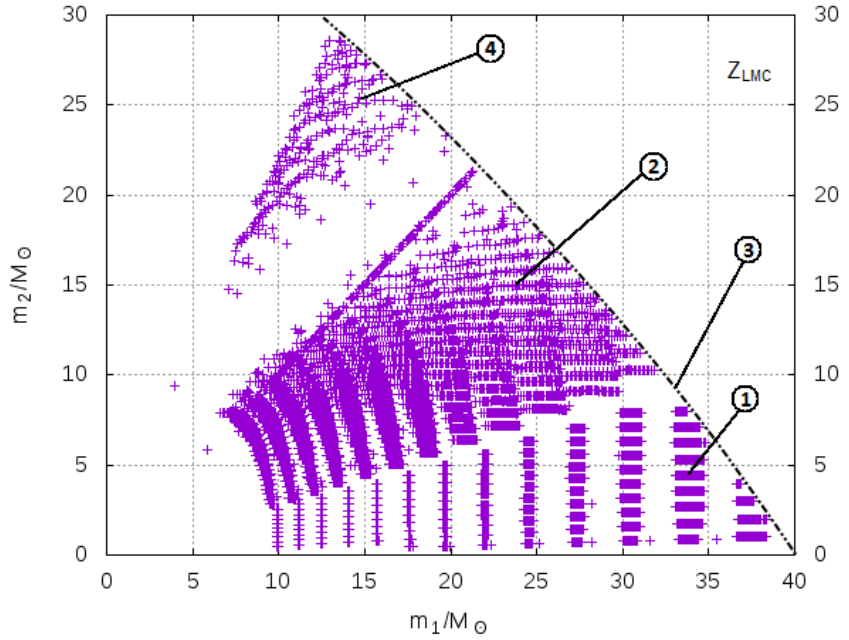

Figure 20: Masses of the primary and secondary star in merger systems at the time of merging. For an explanation of the labels see text.

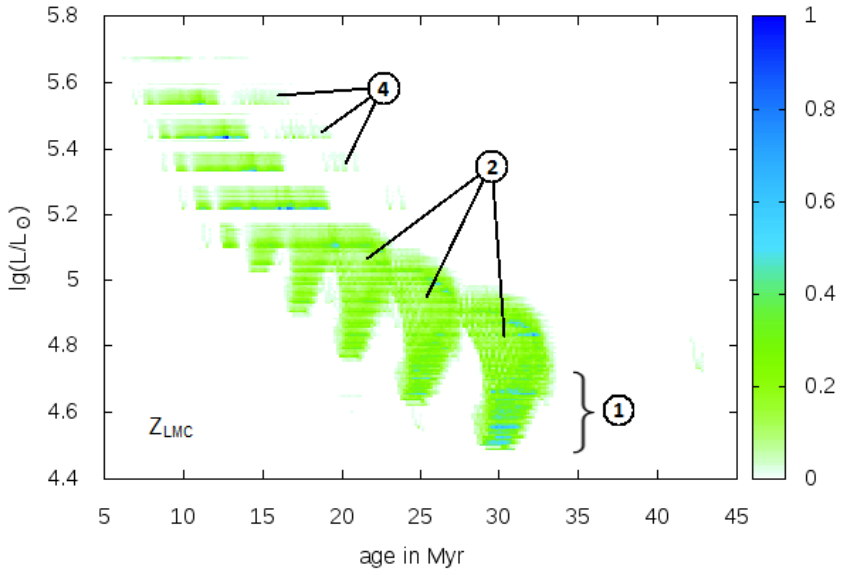

Figure 21: Density map of the luminosity-age dependence on the red giant branch. Depicted are only merger systems. The density index is limited to 1 for better visibility of faint features. For an explanation of the labels see text.

and itemized in the following:

- 1: This region contains the systems which did not undergo mass transfer before merging. The discretisation of M_1 is clearly visible even though the primary stars lose some mass before merging due to stellar winds. The gaps in each column are consistent with the discretisation of initial mass ratio q for each primary mass, which indicates that there is no mass transferred to the secondary star. This region is the most populated in both plots.

- 2: These systems undergo mass transfer before merging. The gaps do not correspond to initial q anymore and the primary stars lose clearly more mass than in the last area. So the secondary star must have accreted mass from the primary and the mass ratio shifts towards higher q.

- 3: This line marks the upper limit of total mass for a system to form a merger product less massive than $40M_\odot$. It does not run exactly on the $M_1 + M_2 = 40M_\odot$ line but a bit above it, because a fraction of the total mass is always lost in the merger process. This line is not visible in Figure 21, because it runs at high luminosities outside of the plot's range.

- 4: In these systems mass transfer occurred before the merger and caused the mass relation to invert, the secondary star becoming the more massive in the binary.

So the shape of the merger models in figure 21 is mainly a result of the discretisation of M_1. Each bulk contains the mergers of one distinct value of M_1. As the rejuvination is stronger for lower binary masses and higher mass ratios (Schneider et. al. 2016) we find the the less massive stars to be at higher ages in the diagram and the uppermost stars (highest q) in each bulk to have the largest horizontal distance to the luminosity curve. The splits in the higher mass bulks are a result of the assigning of merger products to closest mass "single star" equivalents.

Britavskiy et al. (2018) suggest in their work that there is a red straggler effect in the red giant branch analogous to blue stragglers at the main sequence turn-off caused by binary mass transfer and merger which "produce more massive and luminous RSG than expected from single star evolution at a given age". We cannot observe such an effect in our interacting binary models, which resemble the non-interacting luminosity curve too closely. But it fits in well with our observation of merger systems which actually form such objects.

The effect of merger stars on the RGB can also be seen in our star clusters from the previous section. Figure 41 to 45 show the contrast of the RGB cut-outs of each cluster with and without mergers. Interacting and non-interacting systems alone form a discrete, almost vertical line in the RGB region. Adding mergers however causes the branch to be populated above this line at clearly higher luminosities, resembling the shape of the RGB in Figure 3. The luminous extent of each cluster's RGB conforms to the luminosity range of the merger bulks in Figure 19.

5 Conclusion

The binary star data grid by Merchant (2016) allowed us to investigate the influence of binary interaction on certain properties of star clusters.
In clusters of constant age we were able to observe an unravelling of the main-sequence turn-off into a total of four branches of which three are caused by binary interactions (Figure 6). Beside a redder turn-off (branch 3) parallel to the actual main-sequence turn-off (branch 1), located at lower temperatures and composed of rapidly rotating secondary stars that have accreted mass before, there turned out to be a pair of branches: A blue one at higher luminosities and temperatures than the turn-off point (branch 2) contributing to the blue straggler effect and a small red one splitting from the parallel turn-off (branch 4). In branch 2 reside stars that have lost their more massive primary companion after several non-conservative mass transfers as well as secondary stars that slowly accrete mass from a less massive and less luminous primary after a fast mass transfer inverted the mass ratio. The latter have turned out to be the companion stars of those located on branch 4, which only contains primary stars. We interpreted these objects as possible Algol variables and suggested comparison with observational data. These features though might be difficult to distinguish in actual cluster HRDs as they are low in intensity compared to the main sequence and the blue branch is overlain by mergers residing in the same region that also contribute to the blue straggler effect. In clusters of constant star formation those features are not visible except the parallel turn-off, which causes a widening of the main sequence (see Figure 2).

Investigation of the luminosity-age dependence on the RGB for constant star formation showed a distinct relation, luminosity decreasing with age following a continuously dropping curve. Binary interaction only has a minor effect on this relation. It widens the curve towards lower luminosities, but the overall appearance is conserved. Mergers however form rejuvinated stars that are more massive and luminous than other stars of the same age and lie clearly above the luminosity curve (see Figure 19), which highly lowers a potential usefulness of the luminosity-age relation for age determination on the red giant branch.

References

[1] Merchant P.; 2016. The impact of tides and mass transfer on the evolution of metal-poor massive binary stars [dissertation]. Rheinischen Friedrich-Wilhelms-Universität Bonn.

[2] Pols, O.R.; 2009. Stellar Structure and evolution.

[3] Schneider, F. R. N.; Podsiadlowski, Ph.; Langer, N.; Castro, N.; Fossati, L.; 2016. Rejuvenation of stellar mergers and the origin of magnetic fields in massive stars. Monthly Notices of the Royal Astronomical Society, Volume 457, Issue 3, p.2355-2365

[4] Sana, H.; de Koter, A.; de Mink, S. E.; Dunstall, P. R.; Evans, C. J.; Hénault-Brunet, V.; Maíz Apellániz, J.; Ramírez-Agudelo, O. H.; Taylor, W. D.; Walborn, N. R.; Clark, J. S.; Crowther, P. A.; Herrero, A.; Gieles, M.; Langer, N.; Lennon, D. J.; Vink, J. S.; 2013. The VLT-FLAMES Tarantula Survey. VIII. Multiplicity properties of the O-type star population. Astronomy & Astrophysics, Volume 550, id.A107, 22 pp.

[5] Sana, H.; de Mink, S. E.; de Koter, A.; Langer, N.; Evans, C. J.; Gieles, M.; Gosset, E.; Izzard, R. G.; Le Bouquin, J.-B.; Schneider, F. R. N.; 2013. Multiplicity of massive O stars and evolutionary implications. 370 Years of Astronomy in Utrecht. Proceedings of a conference held 2-5 April, 2012 at Hotel Leeuwenhorst, Noordwijkerhout, The Netherlands. ASP Conference Series, Vol. 470. San Francisco: Astronomical Society of the Pacific, 2013., p.141

[6] Britavskiy, N.; Lennon, D.J.; Patrick, L.R.; Evans, C.J.; Herrero, A.; Langer, N.; 2018. The VLT-FLAMES Tarantula Survey. XXIX. Physical parameters of red supergiants in 30 Doradus. Unpublished manuscript.

[7] D'Antona, F.; Milone, A. P.; Tailo, M.; Ventura, P.; Vesperini, E.; di Criscienzo, M.; 2017. Stars caught in the braking stage in young Magellanic Cloud clusters. Nature Astronomy, Volume 1, id. 0186 (2017).

[8] Milone, A. P.; Marino, A. F.; Di Criscienzo, M.; D'Antona, F.; Bedin, L. R.; Da Costa, G.; Piotto, G.; Tailo, M.; Dotter, A.; Angeloni, R.; Anderson, J.; Jerjen, H.; Li, C.; Dupree, A.; Granata, V.; Lagioia, E. P.; Mackey, A. D.; Nardiello, D.; Vesperini, E.; 2018. Multiple stellar populations in Magellanic Cloud clusters - VI. A survey of multiple sequences and Be stars in young clusters. Monthly Notices of the Royal Astronomical Society, Volume 477, Issue 2, p.2640-2663

[9] Erdem, A.; Öztürk, O.; 2014. Non-conservative mass transfers in Algols. Monthly Notices of the Royal Astronomical Society, Volume 441, Issue 2, p.1166-1176

[10] Chen, W.; Li, X.; Qian, S.; 2006. Orbital Evolution of Algol Binaries with a Circumbinary Disk. The Astrophysical Journal, Volume 649, Issue 2, pp. 973-978.

[11] Kopal, Z.; 1955. The classification of close binary systems. Annales d'Astrophysique, Vol. 18, p.379

[12] Sollima, A.; Lanzoni, B.; Beccari, G.; Ferraro, F. R.; Fusi Pecci, F.; 2008. The correlation between blue straggler and binary fractions in the core of Galactic globular clusters. Astronomy and Astrophysics, Volume 481, Issue 3, 2008, pp.701-704

A Tables

age in Myr	$\Delta \log(L/L_\odot)$
6	4.9-5.0
12	4.35-4.45
18	3.9-4.0
24	3.6-3.7
30	3.6-3.7

Table 1: Luminosity ranges for the branches 1, 3 and 4 (see Figure 6) in the histograms in Figures 7, 8, 10 and 11. In these intervals branches 1 and 3 become vertical.

age in Myr	$\Delta \log(L/L_\odot)$
6	5.3-5.2
12	4.6-4.7
18	4.3-4.4
24	4.1-4.2
30	3.9-4.0

Table 2: Luminosity ranges for branch 2 (see Figure 6) in the histogram in Figure 9. In these intervals branch 2 becomes vertical.

Position in branch 2	Sample number	$\log(M_1/\mathrm{M}_\odot)$	q	$\log(P/\mathrm{d})$
parallel to the turn-off	1	1.500	0.275	0.150
	2	1.450	0.275	0.200
	3	1.500	0.350	0.200
	4	1.550	0.275	0.200
	5	1.550	0.400	0.250
	6	1.550	0.475	0.200
clump	1	1.200	0.875	0.250
	2	1.200	0.950	0.250
	3	1.250	0.900	0.300
	4	1.250	0.975	0.325
	5	1.150	0.825	0.175
	6	1.150	0.775	0.175

Table 3: Sample stars of components of branch 2 (see Figure 6). These samples are located in the respective region of the branch at the age of 10Myr. The regions can be seen in Figure 15 and 16.

B Pictures

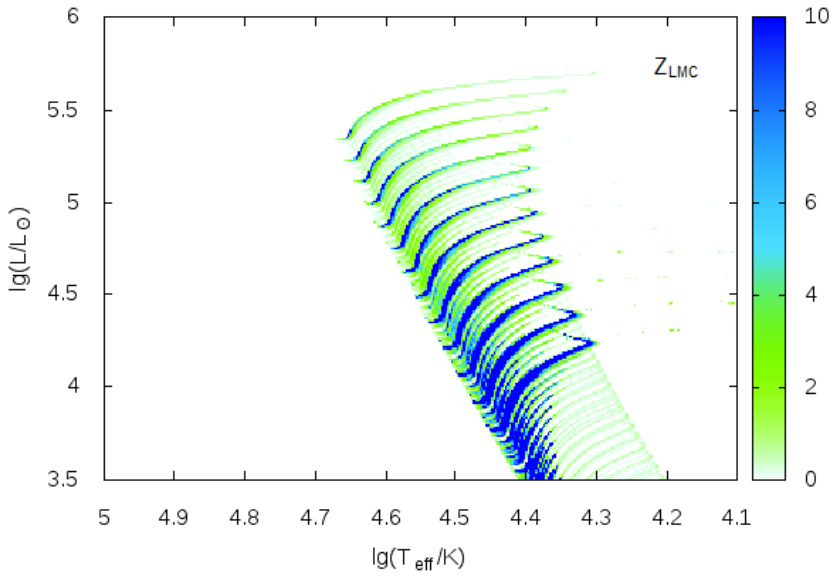

Figure 22: Hertzsprung-Russell diagram as a density map for constant star formation, containing only non-interacting systems. Depicted is the upper end of the main-sequence. All models are weighted according to section 3.3. The density index is limited to 10 for better visibility of faint features.

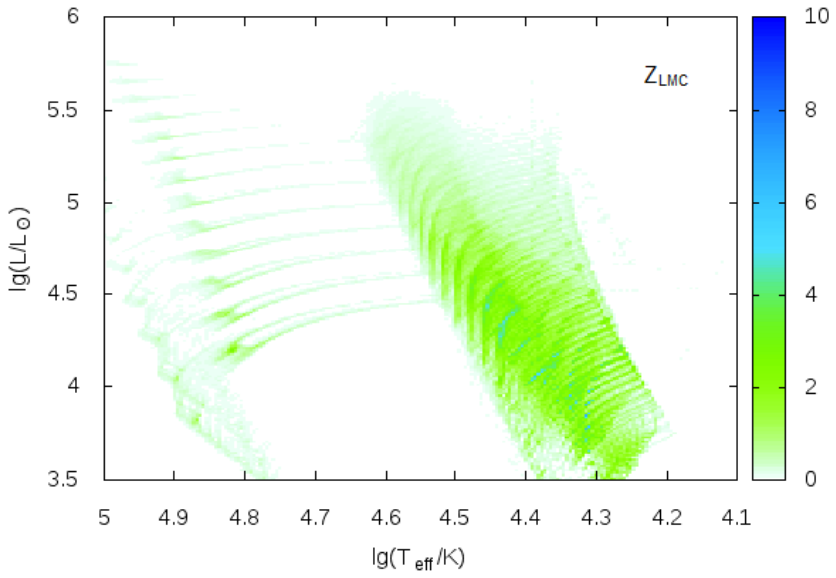

Figure 23: Hertzsprung-Russell diagram as a density map for constant star formation, containing only interacting systems. Depicted is the upper end of the main-sequence. All models are weighted according to section 3.3. The density index is limited to 10 for better visibility of faint features.

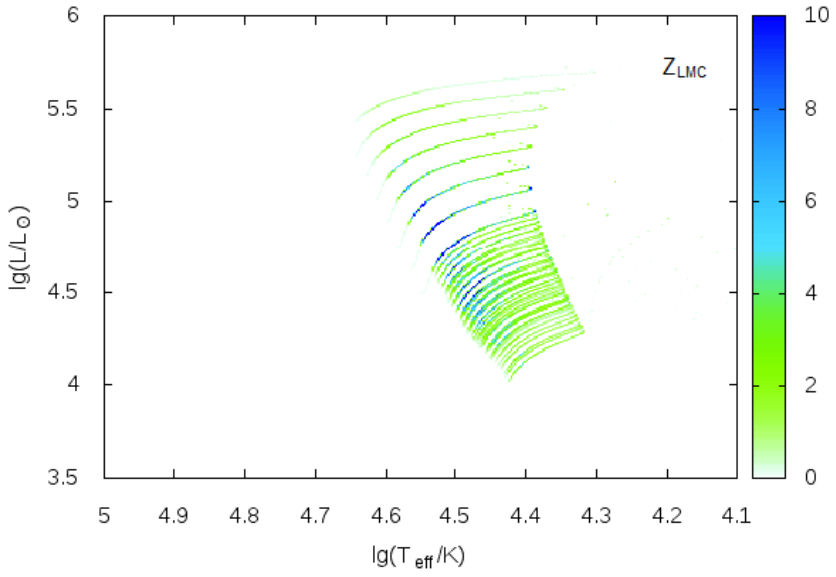

Figure 24: Hertzsprung-Russell diagram as a density map for constant star formation, containing only mergers. Depicted is the upper end of the main-sequence. All models are weighted according to section 3.3. The density index is limited to 10 for better visibility of faint features.

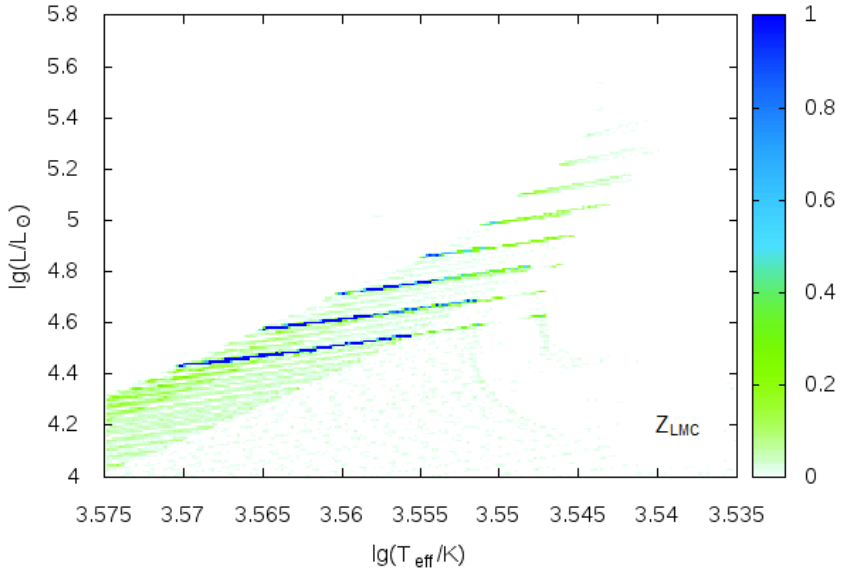

Figure 25: Hertzsprung-Russell diagram as a density map for constant star formation, containing only non-interacting systems. Depicted is the upper end of the red giant branch. All models are weighted according to section 3.3. The density index is limited to 10 for better visibility of faint features.

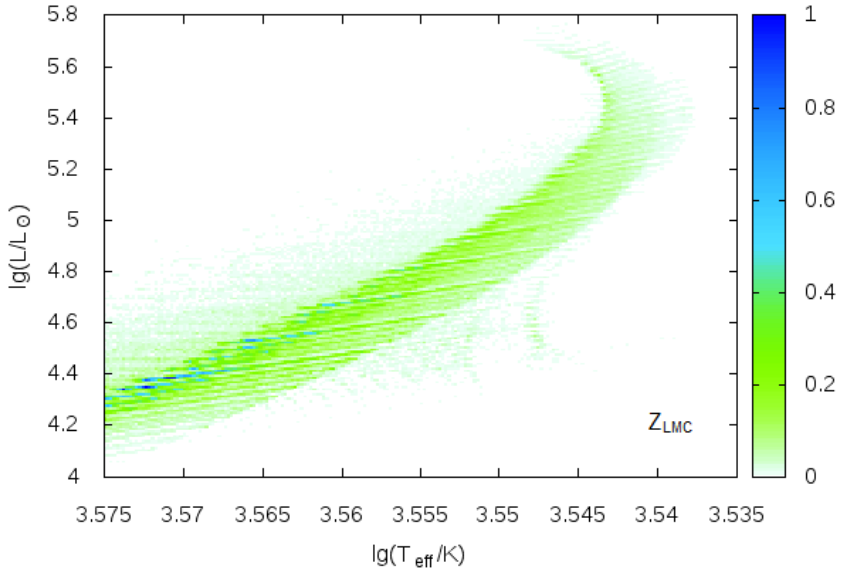

Figure 26: Hertzsprung-Russell diagram as a density map for constant star formation, containing only interacting systems. Depicted is the upper end of the red giant branch. All models are weighted according to section 3.3. The density index is limited to 10 for better visibility of faint features.

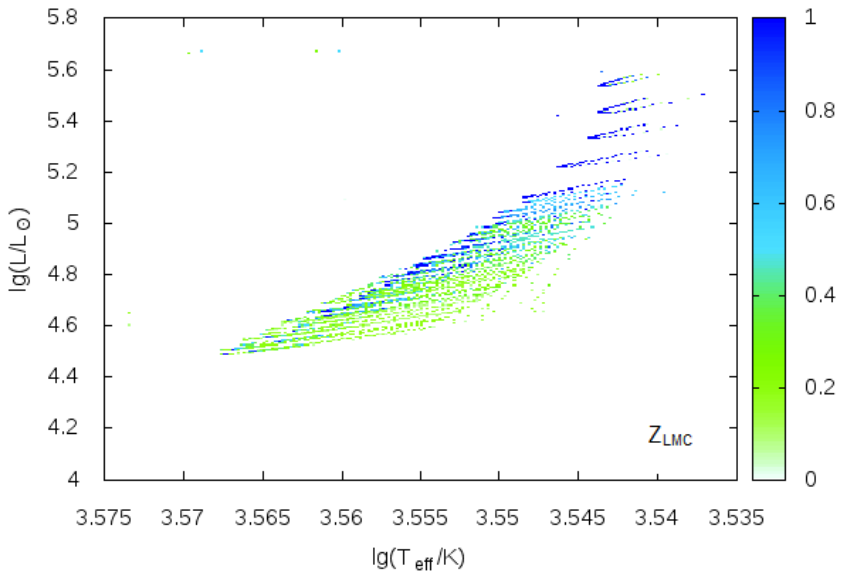

Figure 27: Hertzsprung-Russell diagram as a density map for constant star formation, containing only mergers. Depicted is the upper end of the red giant branch. All models are weighted according to section 3.3. The density index is limited to 10 for better visibility of faint features.

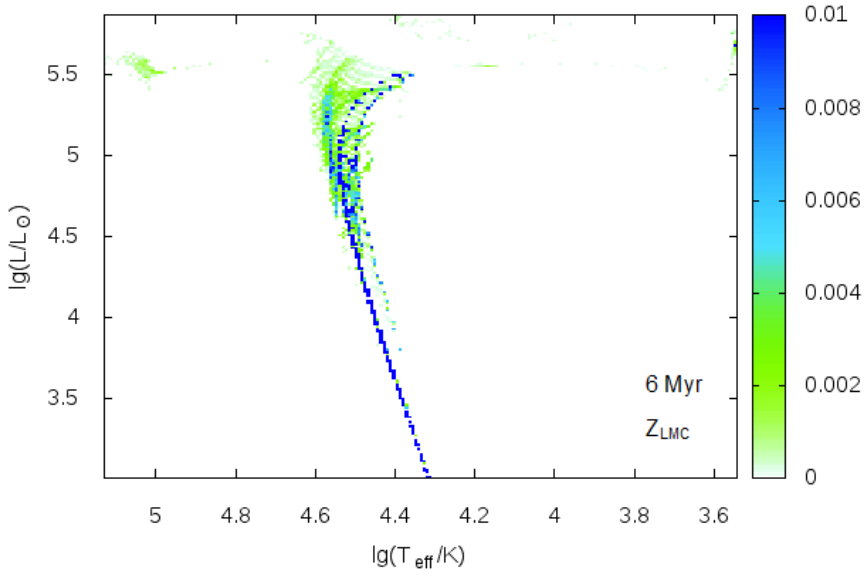

Figure 28: Hertzsprung-Russell diagram as a density map of the main-sequence turn-off of a star cluster at constant age 6Myr, containing interacting and non-interacting systems. All models are weighted according to section 3.3. The density index is limited to 0.01 for better visibility of faint features.

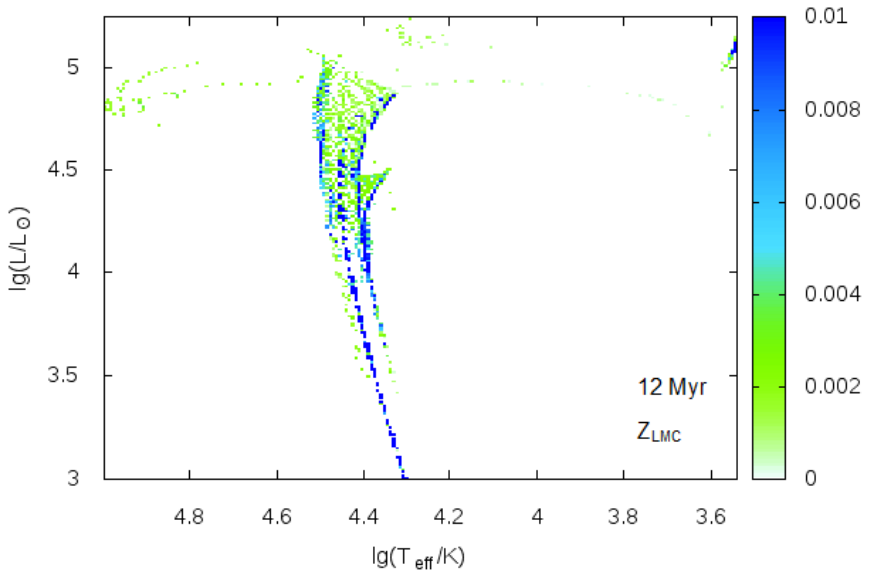

Figure 29: Hertzsprung-Russell diagram as a density map of the main-sequence turn-off of a star cluster at constant age 12Myr, containing interacting and non-interacting systems. All models are weighted according to section 3.3. The density index is limited to 0.01 for better visibility of faint features.

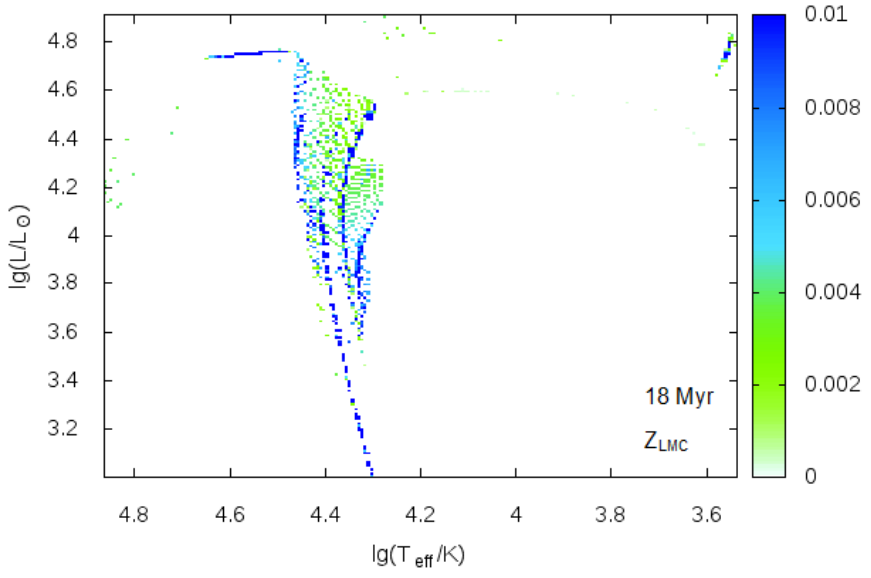

Figure 30: Hertzsprung-Russell diagram as a density map of the main-sequence turn-off of a star cluster at constant age 18Myr, containing interacting and non-interacting systems. All models are weighted according to section 3.3. The density index is limited to 0.01 for better visibility of faint features.

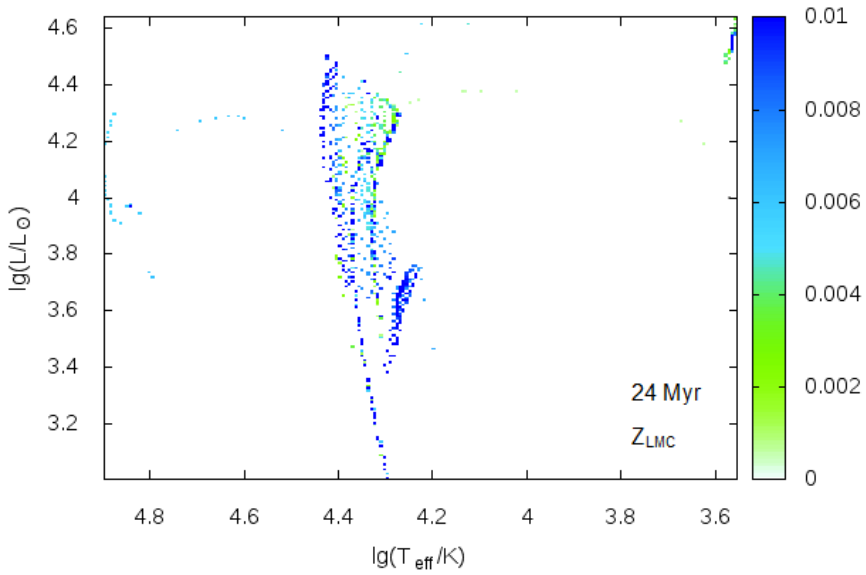

Figure 31: Hertzsprung-Russell diagram as a density map of the main-sequence turn-off of a star cluster at constant age 24Myr, containing interacting and non-interacting systems. All models are weighted according to section 3.3. The density index is limited to 0.01 for better visibility of faint features.

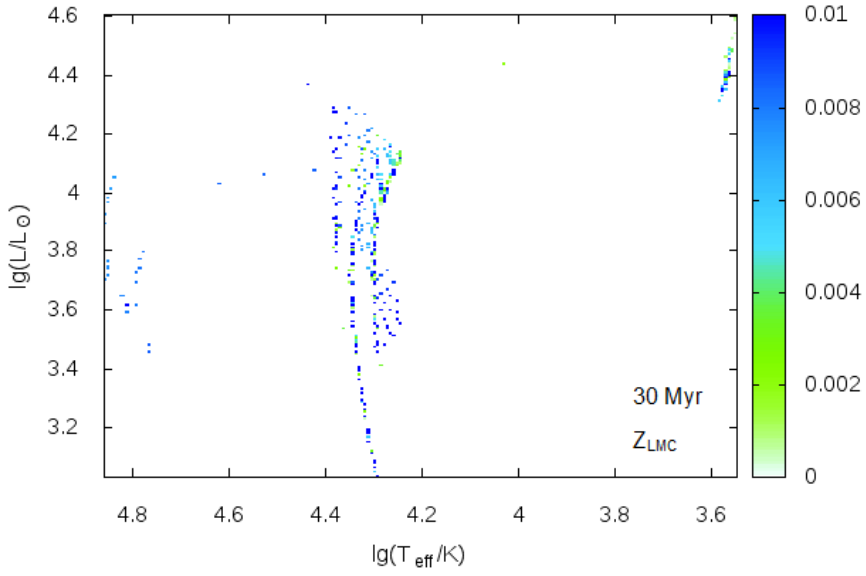

Figure 32: Hertzsprung-Russell diagram as a density map of the main-sequence turn-off of a star cluster at constant age 30Myr, containing interacting and non-interacting systems. All models are weighted according to section 3.3. The density index is limited to 0.01 for better visibility of faint features.

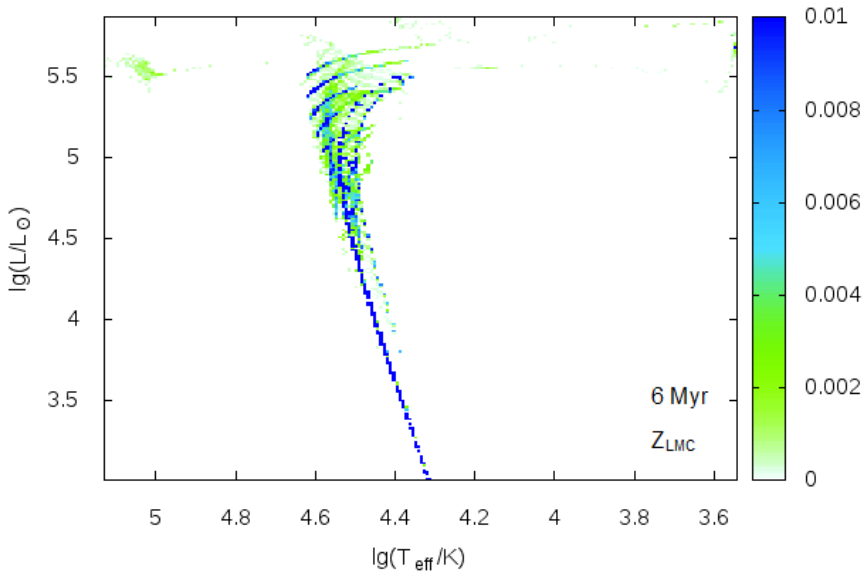

Figure 33: Hertzsprung-Russell diagram as a density map of the main-sequence turn-off of a star cluster at constant age 6Myr, containing interacting systems, non-interacting systems and mergers. All models are weighted according to section 3.3. The density index is limited to 0.01 for better visibility of faint features.

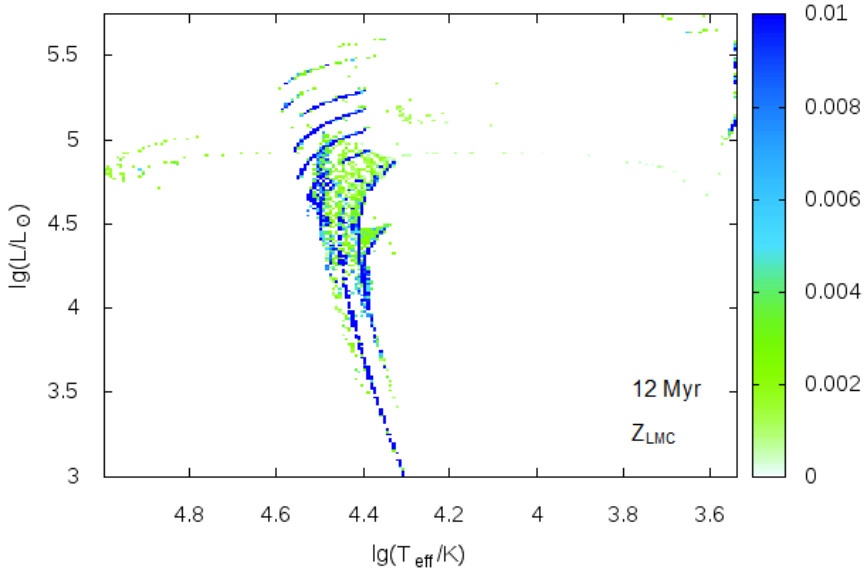

Figure 34: Hertzsprung-Russell diagram as a density map of the main-sequence turn-off of a star cluster at constant age 12Myr, containing interacting systems, non-interacting systems and mergers. All models are weighted according to section 3.3. The density index is limited to 0.01 for better visibility of faint features.

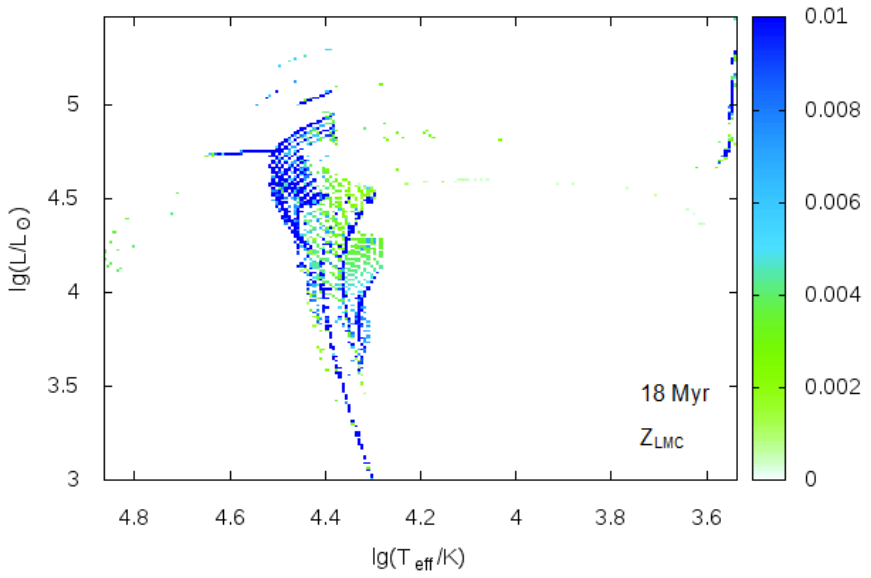

Figure 35: Hertzsprung-Russell diagram as a density map of the main-sequence turn-off of a star cluster at constant age 18Myr, containing interacting systems, non-interacting systems and mergers. All models are weighted according to section 3.3. The density index is limited to 0.01 for better visibility of faint features.

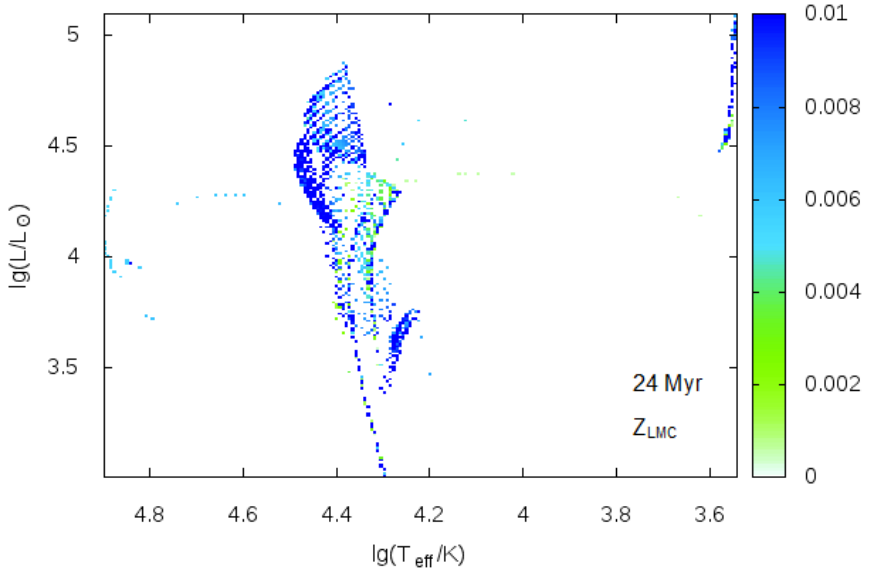

Figure 36: Hertzsprung-Russell diagram as a density map of the main-sequence turn-off of a star cluster at constant age 24Myr, containing interacting systems, non-interacting systems and mergers. All models are weighted according to section 3.3. The density index is limited to 0.01 for better visibility of faint features.

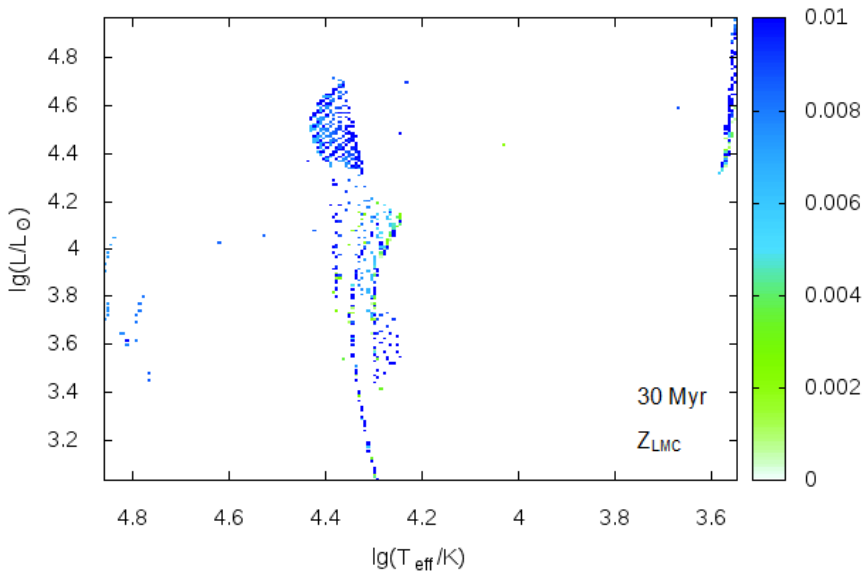

Figure 37: Hertzsprung-Russell diagram as a density map of the main-sequence turn-off of a star cluster at constant age 30Myr, containing interacting systems, non-interacting systems and mergers. All models are weighted according to section 3.3. The density index is limited to 0.01 for better visibility of faint features

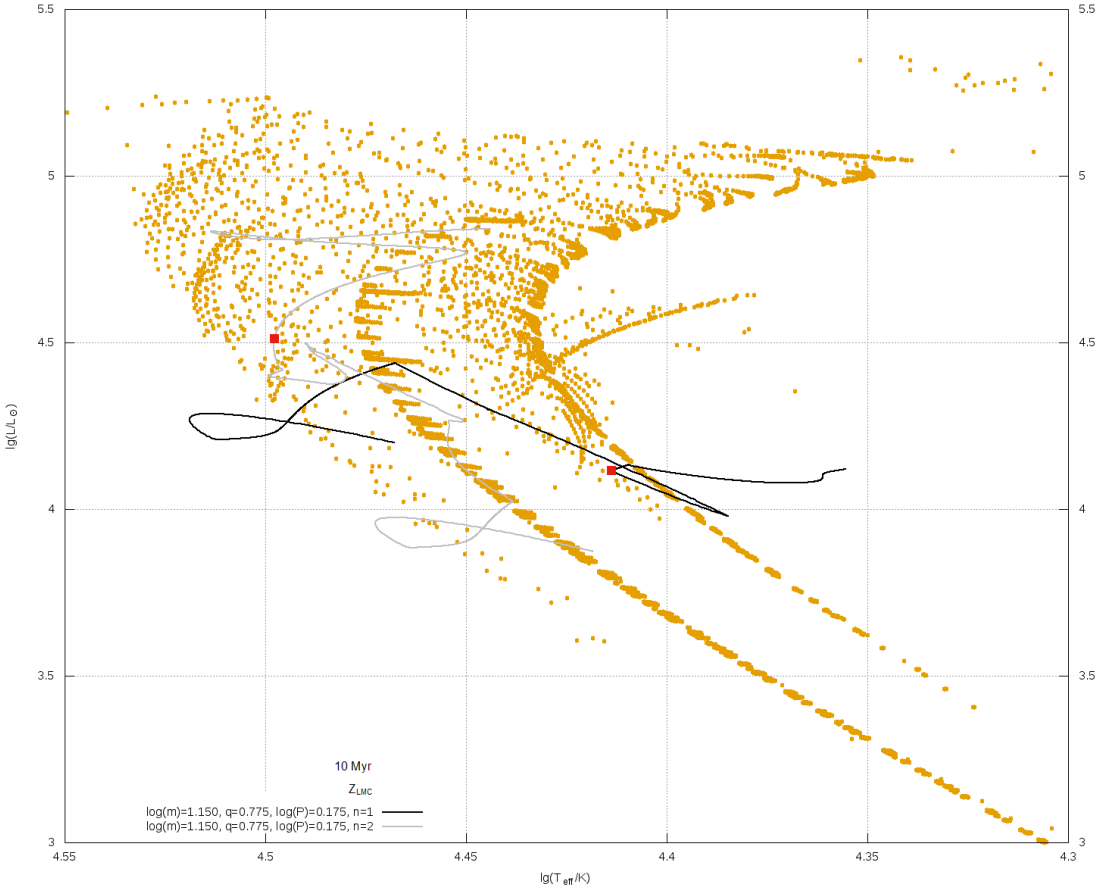

Figure 38: Hertzsprung-Russell diagram as a scatterplot of the main-sequence turn-off of a star cluster at constant age 10Myr, containing interacting and non-interacting systems. Additionally depicted are the evolutionary tracks of the binary pair $\log(M_1/\mathrm{M}_\odot) = 1.150$, $q = 0.775$, $\log(P/\mathrm{d}) = 0.175$. Their positions at the time of the cluster age are marked by red squares.

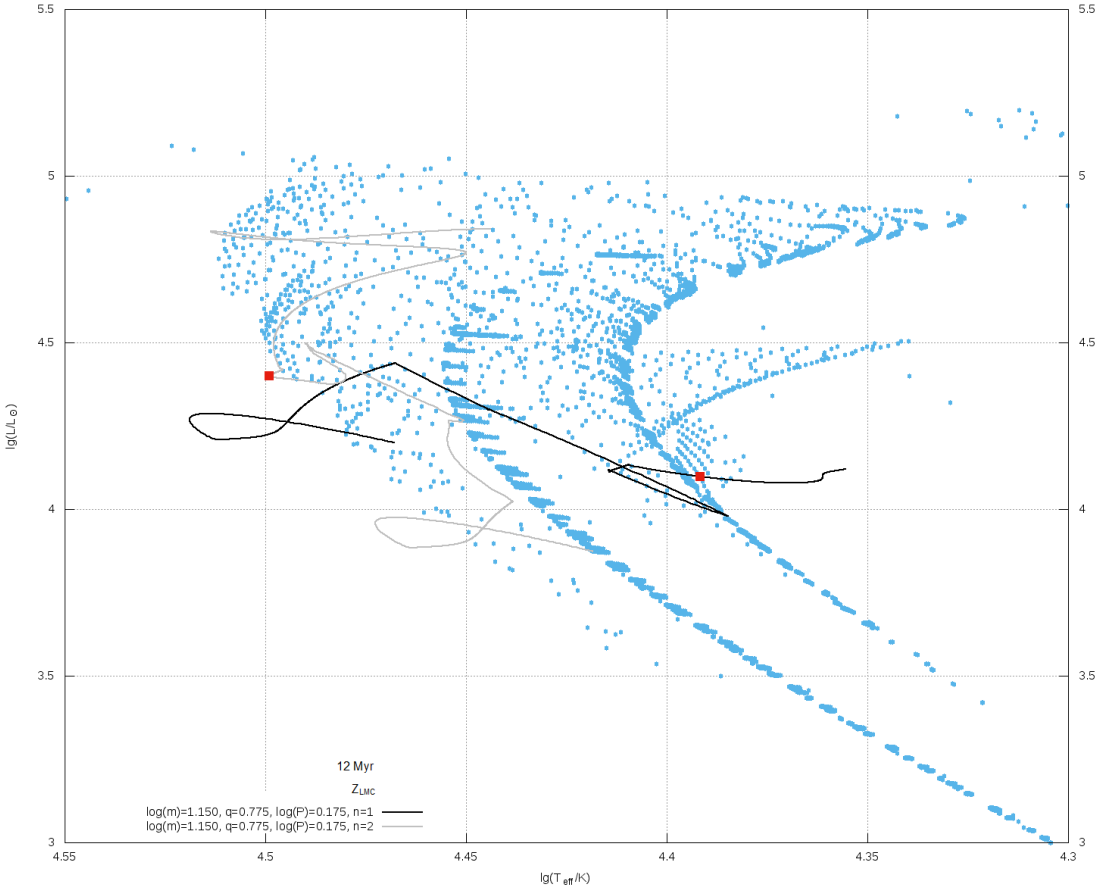

Figure 39: Hertzsprung-Russell diagram as a scatterplot of the main-sequence turn-off of a star cluster at constant age 12Myr, containing interacting and non-interacting systems. Additionally depicted are the evolutionary tracks of the binary pair $\log(M_1/\mathrm{M}_\odot) = 1.150$, $q = 0.775$, $\log(P/\mathrm{d}) = 0.175$. Their positions at the time of the cluster age are marked by red squares.

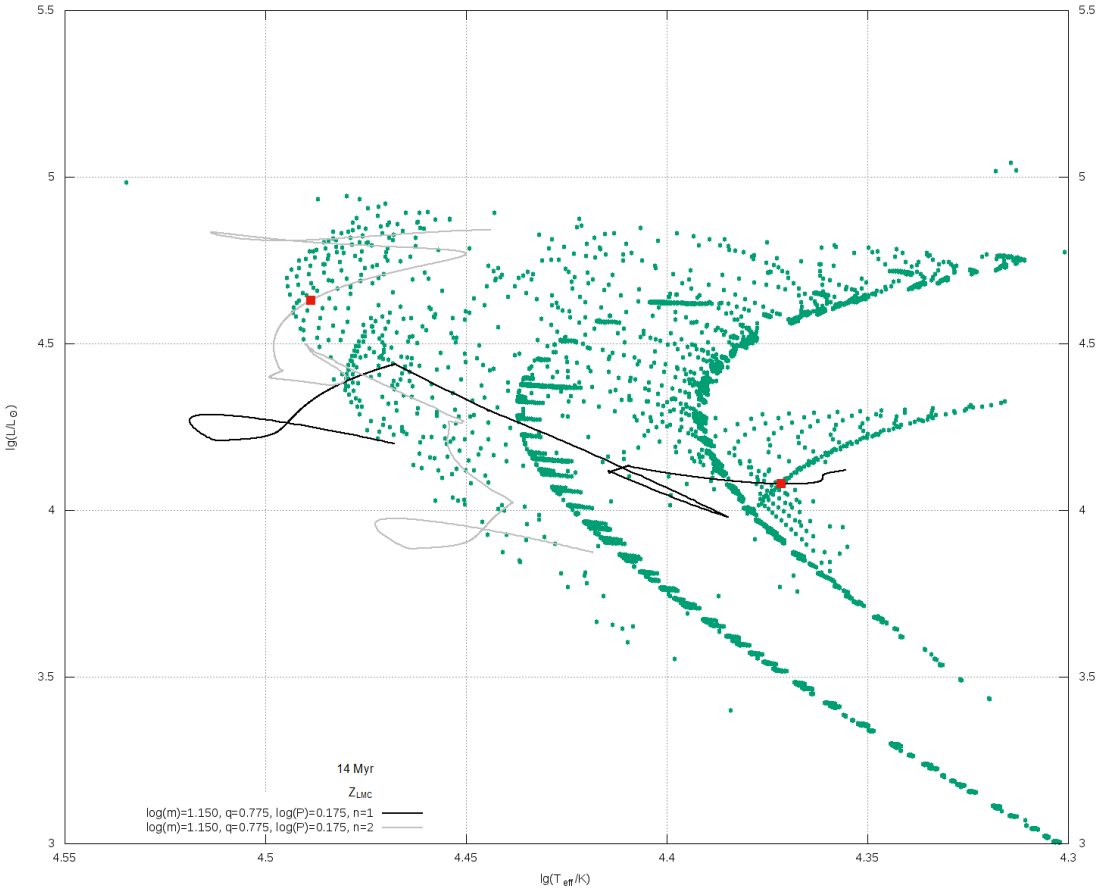

Figure 40: Hertzsprung-Russell diagram as a scatterplot of the main-sequence turn-off of a star cluster at constant age 14Myr, containing interacting and non-interacting systems. Additionally depicted are the evolutionary tracks of the binary pair $\log(M_1/\mathrm{M}_\odot) = 1.150$, $q = 0.775$, $\log(P/\mathrm{d}) = 0.175$. Their positions at the time of the cluster age are marked by red squares.

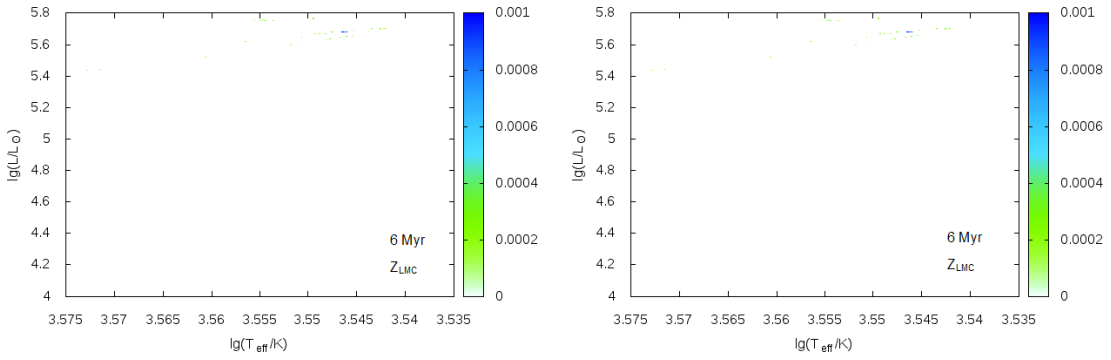

Figure 41: Hertzsprung-Russell diagrams as desity maps for the red giant branch of a star cluster of the constant age 6Myr. The left picture contains interacting and non-interacting systems. The right picture additionally contains mergers. All models are weighted according to section 3.3. The density index is limited to 0.001 for better visibility of faint features.

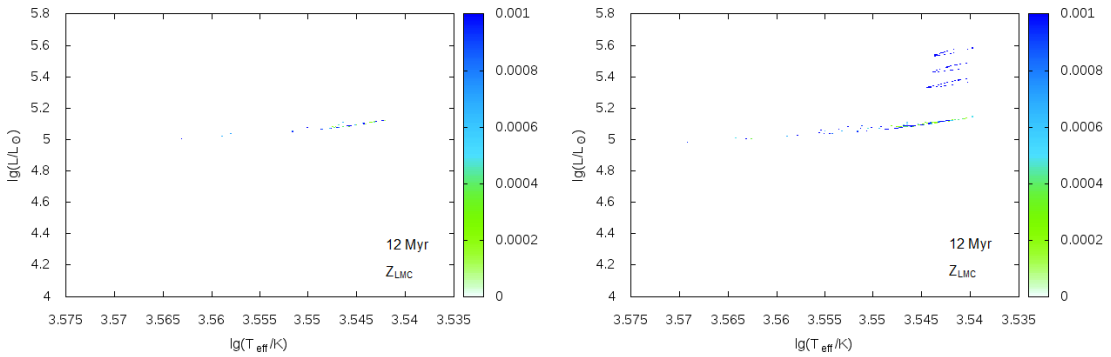

Figure 42: Hertzsprung-Russell diagrams as desity maps for the red giant branch of a star cluster of the constant age 12Myr. The left picture contains interacting and non-interacting systems. The right picture additionally contains mergers. All models are weighted according to section 3.3. The density index is limited to 0.001 for better visibility of faint features.

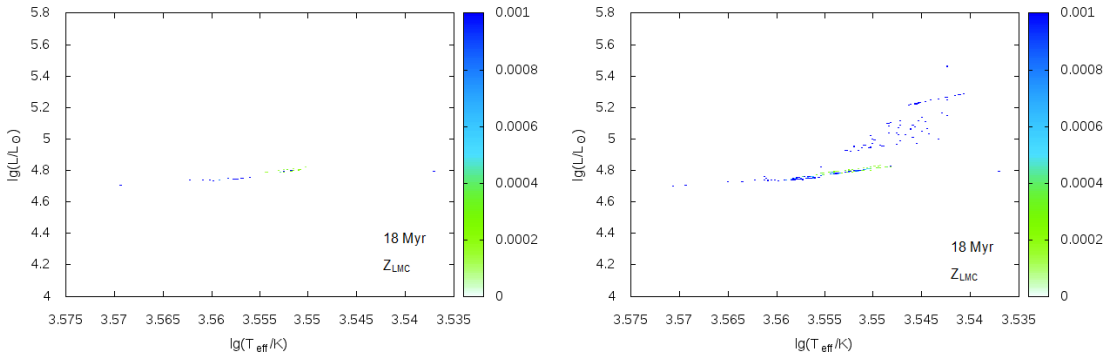

Figure 43: Hertzsprung-Russell diagrams as desity maps for the red giant branch of a star cluster of the constant age 18Myr. The left picture contains interacting and non-interacting systems. The right picture additionally contains mergers. All models are weighted according to section 3.3. The density index is limited to 0.001 for better visibility of faint features.

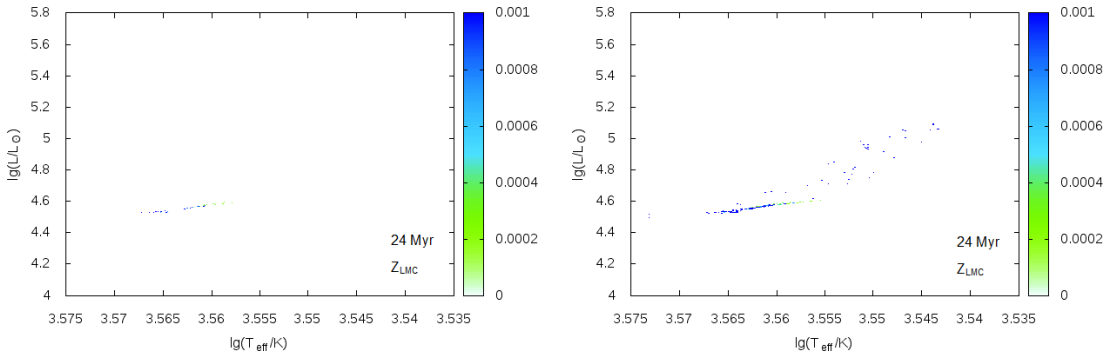

Figure 44: Hertzsprung-Russell diagrams as desity maps for the red giant branch of a star cluster of the constant age 24Myr. The left picture contains interacting and non-interacting systems. The right picture additionally contains mergers. All models are weighted according to section 3.3. The density index is limited to 0.001 for better visibility of faint features.

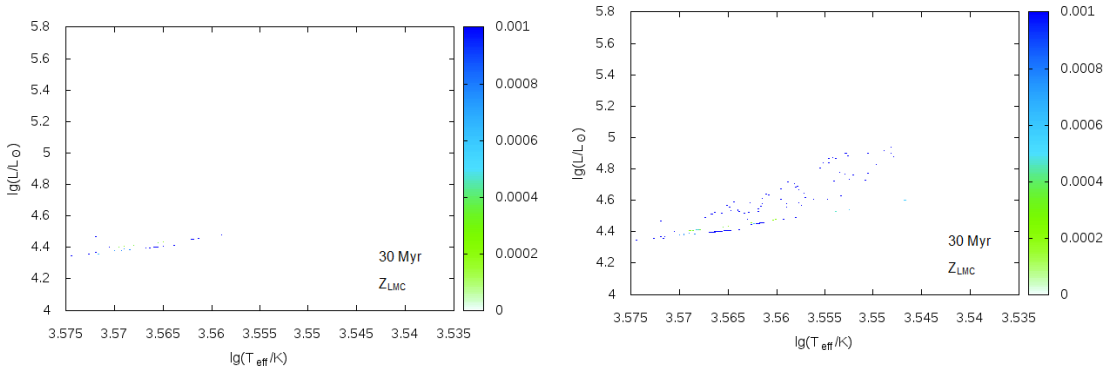

Figure 45: Hertzsprung-Russell diagrams as desity maps for the red giant branch of a star cluster of the constant age 30Myr. The left picture contains interacting and non-interacting systems. The right picture additionally contains mergers. All models are weighted according to section 3.3. The density index is limited to 0.001 for better visibility of faint features.